Model-Predictive Control of Multilevel Inverters: Challenges, Recent Advances, and Trends

Ibrahim Harbi, *Member, IEEE*, Jose Rodriguez, *Life Fellow, IEEE*, Eyke Liegmann, *Student Member, IEEE*, Hamza Makhamreh, Marcelo Lobo Heldwein, *Senior Member, IEEE*, Mateja Novak, *Member, IEEE*, Mattia Rossi, *Member, IEEE*, Mohamed Abdelrahem, *Senior Member, IEEE*, Mohamed Trabelsi, *Senior Member, IEEE*, Mostafa Ahmed, *Member, IEEE*, Petros Karamanakos, *Senior Member, IEEE*, Shuai Xu, *Member, IEEE*, Tomislav Dragičević, *Senior Member, IEEE*, and Ralph Kennel, *Senior Member, IEEE*

***Abstract*—Model-predictive control (MPC) has emerged as a promising control method in power electronics, particularly for multiobjective control problems such as multilevel inverter (MLI) applications. Over the past two decades, improving the performance of MPC and tackling its technical challenges, such as computational load, modeling accuracy, cost function design, and weighting factor selection, have attracted great interest in power electronics. This article aims to discuss the current state of MPC strategies for MLI applications, describing the significance of each challenge with the reported effective solutions. Through this review, the MPC methods are categorized into two groups: direct MPC (without modulator) and indirect MPC (with modulator). The recent advances of each category are presented and analyzed, focusing on direct MPC as the most applied method for MLI topologies. In addition, some of the important concepts are experimentally validated through a case study and compared under the same operating conditions to evaluate the performance and highlight their features. Finally, the future trends of MPC for MLI applications are discussed based on the current state and reported developments.**

***Index Terms*—Capacitor balance, current control, dc-link balance, model-predictive control (MPC), multilevel inverter (MLI).**

Manuscript received 12 December 2022; revised 18 May 2023; accepted 13 June 2023. Date of publication 22 June 2023; date of current version 28 July 2023. The work of Jose Rodriguez was supported by the Chilean National Agency for Research and Development under Grants FB0008, 1210208, and 1221293. Recommended for publication by Associate Editor M. Perez. *(Corresponding author: Ibrahim Harbi.)*

Ibrahim Harbi is with the Chair of High-Power Converter Systems, Technical University of Munich, 80333 Munich, Germany, and also with the Department of Electrical Engineering, Faculty of Engineering, Menoufia University, Shebin El-Koum 32511, Egypt (e-mail: ibrahim.harbi@tum.de).

Jose Rodriguez is with the Faculty of Engineering, Universidad San Sebastian, Santiago 8420524, Chile (e-mail: jose.rodriguezp@uss.cl).

Eyke Liegmann, Marcelo Lobo Heldwein, Mohamed Abdelrahem, Mostafa Ahmed, and Ralph Kennel are with the Chair of High-Power Converter Systems, Technical University of Munich, 80333 Munich, Germany (e-mail: eyke.liegmann@tum.de; marcelo.heldwein@tum.de; mohamed.abdelrahem@tum.de; mostafa.ahmed@tum.de; ralph.kennel@tum.de).

Hamza Makhamreh is with the Department of Electrical and Electronics Engineering, Özyeğin University, 34794 Istanbul, Turkey (e-mail: hamza.makhamreh@ozyegin.edu.tr).

Mateja Novak is with the AAU Energy, Aalborg University, 9220 Aalborg, Denmark (e-mail: nov@energy.aau.dk).

Mattia Rossi and Petros Karamanakos are with the Faculty of Information Technology and Communication Sciences, Tampere University, 33101 Tampere, Finland (e-mail: mattia.rossi@ieee.org; p.karamanakos@ieee.org).

Mohamed Trabelsi is with the Department of Electronics and Communications Engineering, Kuwait College of Science and Technology, Kuwait City 27235, Kuwait (e-mail: m.trabelsi@kcst.edu.kw).

Shuai Xu is with the State Key Laboratory of Rail Transit Vehicle System, Southwest Jiaotong University, Chengdu 610031, China (e-mail: sxu@swjtu.edu.cn).

Tomislav Dragičević is with the Department of Electrical Engineering, Technical University of Denmark, 2800 Lyngby, Denmark (e-mail: tomdr@elektro.dtu.dk).

Color versions of one or more figures in this article are available at https://doi.org/10.1109/TPEL.2023.3288499.

Digital Object Identifier 10.1109/TPEL.2023.3288499

I. Introduction

Owing to their advantages of limited voltage stress on semiconductor devices, low switching losses, and reduced high-frequency emissions, multilevel inverters (MLIs) have been considered appealing solutions for medium-/high-voltage high-power applications [1], [2]. In addition, MLIs are also potentially attractive for low-voltage/power applications to avert the fundamental problems of conventional two-level (2L) inverters, namely high switching loss, large filter dimensions, and electromagnetic interference [3].

Typically, the control of MLIs is a challenging and multiobjective task, e.g., current control, and internal voltages regulations, which motivated the research community to consider advanced control strategies. Among them, model-predictive control (MPC) has proven to be a promising control method for power converters in general and MLIs in particular. Although MPC was first introduced in the 1960s [4], its investigations into power electronic systems started in the 1980s and its actual popularity emerged in the 2000s as a result of massive technological advances in digital platforms [5], [6], [7]. The industrial implementation of MPC has been realized by ABB Ltd. in some products, such as ACS2000 for medium-voltage (MV) drives [8]. MPC offers several advantages such as simplicity of design, high dynamic performance, and the ability to include the constraints and nonlinearities of the system in a straightforward way [7]. In addition, an outstanding feature of MPC is the capability to handle multiple control objectives using a well-designed cost function in conjunction with constraints. Therefore, it has been widely applied to different MLI topologies in various application areas such as neutral-point-clamped (NPC) converter in MV grid-connected applications [9], flying capacitor (FC) converter

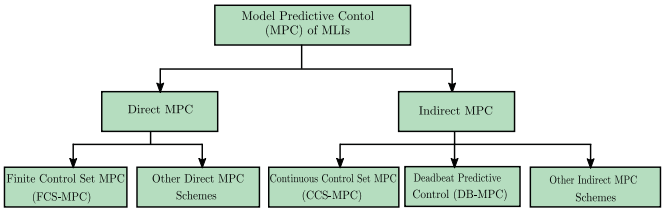

Fig. 1. Classification of MPC methods applied to multilevel inverters.

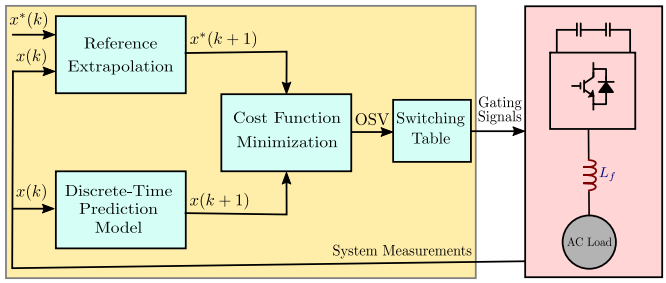

Fig. 2. Block diagram of standard FCS-MPC.

in active power filter [10], cascaded H-bridge (CHB) converter in renewable energy systems [11], and five-level active NPC (5L-ANPC) converter in electrical drives [12], to name a few.

In general, MPC uses the model of the system under control to predict its behavior in a defined prediction horizon. Then, using a cost function that defines the system objectives, the control action is determined by minimizing the errors between the predicted and reference values. The output of the MPC is a sequence of control actions in each control cycle, but only the first action is applied. Several MPC schemes have been reported in the literature for MLIs. According to the output of the optimization problem, MPC methods can be categorized into two groups, i.e., direct MPC and indirect MPC, as shown in Fig. 1. In direct MPC, the controller action is an integer vector and is applied directly to the system without the need for a modulation stage, i.e., the controller outputs the switching signals. In indirect MPC, the MPC controller outputs the control action as a real-valued vector, and then, a modulator is used to generate the switching pulses.

Considering the first category, direct MPC, finite-control-set MPC (FCS-MPC) is considered the most popular MPC scheme in MLI applications. FCS-MPC has the ability to directly exploit the discrete nature of the power converters. By evaluating the finite converter states in a cost function containing the control objectives, the optimal control action can be identified [13]. One prominent merit of FCS-MPC is the ease of solving the control problem, even when there are multiple control objectives and system constraints. However, the required online calculations for variable predictions and cost function minimization increase the computational burden, especially for high-level MLIs. In addition, variable switching frequency, tuning of weighting factors (WFs), and long-horizon implementation are considered challenges in FCS-MPC [7], [13], [14], [15], [16], [17]. Several developments and improvements have recently been reported to compensate for these disadvantages, which will be discussed in this article.

In contrast to direct MPC, where control and modulation take place in one computational stage, indirect MPC solves these problems in a sequential manner. Hence, indirect MPC computes the control action, e.g., the modulating signal or the duty ratio, which is subsequently fed into a modulator for the generation of the switching commands. Continuous-control-set MPC (CCS-MPC) methods are the most common in this category, where the optimization problem is formulated as a constrained or unconstrained quadratic program (QP). Although the latter has higher computational load, it is relatively modest compared to FCS-MPC because the computational cost does not rely on the number of levels in MLI topologies, and part of the optimization problem is solved offline [18], [19]. However, constructing the linear system model for the CCS-MPC is not an easy task, especially for the MLI topologies, which are typically bilinear systems [18].

Generally, any MPC scheme has three key phases, namely the prediction model, cost function, and optimization method. Each phase has relevant issues and limitations that represent research points in the academic community. In this regard, several works have recently been proposed for MLI applications. Accordingly, and considering the most common MPC methods for MLIs in Fig. 1, this article summarizes the recent advances reported in the literature to address these challenges and discusses future trends. Moreover, some of the important concepts are validated by the experimental implementation and compared with the standard MPC method.

The rest of this article is organized as follows. Section II describes the design steps of the FCS-MPC, considering the grid-connected 5L-ANPC converter as a case study. The importance of each FCS-MPC challenge and the reported effective solutions is provided in Section III. Section IV deals with other popular direct MPC methods, such as Lyapunov-based MPC. Indirect MPC methods for MLIs, including CCS-MPC and deadbeat MPC (DB-MPC), are covered in Section V. Section VIII discusses the future trends of MPC for MLI applications. Finally, Section IX concludes this article.

II. Finite-Control-Set MPC

Fig. 2 shows the block diagram of the standard FCS-MPC strategy with a short (one-step) prediction horizon ($N_p = 1$). The design and operating principles can be summarized in three steps as follows:

1) constructing a discrete-time prediction model;
2) designing the cost function that includes the control objectives and constraints;
3) defining and applying the optimal vector that has a minimal cost function through the optimization algorithm.

The analysis presented here is based on the well-known 5L-ANPC inverter connected to the grid, as shown in Fig. 3. Besides the primary current tracking objective, FC balancing and neutral-point (NP) potential control are two control targets that need to be considered in the 5L-ANPC inverter. The description and operating principles of the considered case study are presented in [20] and [21].

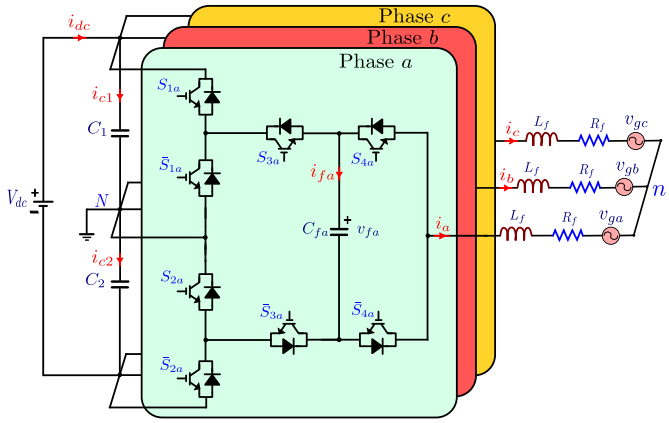

Fig. 3. Circuit configuration of the grid-connected 5L-ANPC converter.

TABLE I
SWITCHING STATES OF PHASE x OF THE 5L-ANPC INVERTER

State	s_{1x}/s_{2x}	s_{3x}	s_{4x}	v_{xN}	i_{fx}
V_1	1	1	1	$V_{\rm dc}/2$	0
V_2	1	1	0	$V_{\rm dc}/4$	i_x
V_3	1	0	1	$V_{\rm dc}/4$	i_x
V_4	1	0	0	0	0
V_5	0	1	1	0	0
V_6	0	1	0	$-V_{\rm dc}/4$	i_x
V_7	0	0	1	$-V_{\rm dc}/4$	i_x
V_8	0	0	0	$-V_{\rm dc}/2$	0

A. Discrete-Time Prediction Model

The predictive model is considered the core of MPC strategies as it is required to predict the future values of the controlled variable. In addition, prediction accuracy is an important issue that significantly affects control performance. Therefore, a time-continuous system model that fully includes the system dynamics should be first built. Referring to the system shown in Fig. 3, the switching states of one leg of the 5L-ANPC inverter are listed in Table I. $x \in \{a, b, c\}$ denotes the respective phase, and the switching function s_{ix} $(i = \{1, 2, 3, 4\})$ of switch S_{ix} is defined as

$$s_{ix} = \begin{cases} 1, & \text{if } S_{ix} \text{ is ON} \\ 0, & \text{if } S_{ix} \text{ is OFF} \end{cases}. \tag{1}$$

According to the inverter switching states, the inverter phase-to-neutral voltage v_{xN} can be expressed as

$$v_{xN} = s_{1x}s_{3x}v_{c1} - \bar{s}_{2x}\bar{s}_{3x}v_{c2} + (s_{4x} - s_{3x})v_{fx} \tag{2}$$

where v_{c1} and v_{c2} are the dc-link voltages and v_{fx} is the voltage of the phase capacitor C_{fx}. The dynamic system equations of the three-phase grid-connected system in the abc-frame are expressed as

$$v_{xN} = R_f i_x + L_f \frac{d}{dt} i_x + v_{gx} + v_{nN} \tag{3}$$

where R_f and L_f are the resistance and inductance of the filter, respectively. v_{gx} is the grid voltage and v_{nN} refers to the common-mode voltage (CMV). To decouple the control loops, the three-phase system is preferably modeled in a 2-D frame, either stationary $\alpha\beta$-frame or rotating dq-frame. In doing so,

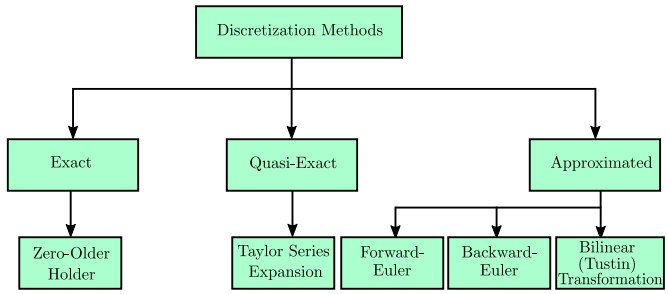

Fig. 4. Classification discretization methods for MPC.

$\mathbf{x}_{abc} = [x_a\ x_b\ x_c]^T$ is transformed to the $\alpha\beta$-frame as

$$\mathbf{x}_{\alpha\beta} = \mathbf{K}\mathbf{x}_{abc} \tag{4}$$

where $\mathbf{K}$ is the transformation matrix and expressed as

$$\mathbf{K} = \frac{2}{3}\begin{bmatrix} 1 & \frac{-1}{2} & \frac{-1}{2} \\ 0 & \frac{\sqrt{3}}{2} & \frac{-\sqrt{3}}{2} \end{bmatrix}. \tag{5}$$

Accordingly, the continuous-time model in (3) can be written in the $\alpha\beta$-frame as

$$\mathbf{v} = R_f\mathbf{i} + L_f\frac{d}{dt}\mathbf{i} + \mathbf{v}_g \tag{6}$$

where $\mathbf{v} = [v_\alpha\ v_\beta]$, $\mathbf{i} = [i_\alpha\ i_\beta]$, and $\mathbf{v}_g = [v_{g\alpha}\ v_{g\beta}]$.

The model of the phase FC (C_{fx}) is built based on the inverter states in Table I as

$$i_{fx} = C_{fx}\frac{d}{dt}v_{fx} = (s_{3x} - s_{4x})i_x \tag{7}$$

where i_{fx} is the current of C_{fx}. Similarly, the dc-link capacitors C_1 and C_2 are modeled as

$$\left.\begin{aligned} i_{c1} = C_1\tfrac{d}{dt}v_{c1} = i_{\rm dc} - \sum_{x\in\{a,b,c\}} s_{1x}s_{3x}i_x \\ i_{c2} = C_2\tfrac{d}{dt}v_{c2} = i_{\rm dc} + \sum_{x\in\{a,b,c\}} \bar{s}_{2x}\bar{s}_{3x}i_x \end{aligned}\right\} \tag{8}$$

where i_{c1} and i_{c2} are the currents of C_1 and C_2, respectively. For identical dc-link capacitors $(C_1 = C_2 = C)$, the dc-link balancing can be formulated as

$$\Delta i_c = C\frac{d}{dt}\Delta v_c = -\sum_{x\in\{a,b,c\}} (s_{1x}s_{3x} + \bar{s}_{2x}\bar{s}_{3x})i_x \tag{9}$$

where $\Delta i_c = i_{c1} - i_{c2}$ and $\Delta v_c = v_{c1} - v_{c2}$. As previously mentioned, MPC implementation is based on the discrete-time models. Therefore, after constructing the continuous-time models, a discretization method should be applied. For the discretization procedure, two important aspects should be taken into account [[22], Ch. 7]. First, the computational load should be low so as not to add heavy computations to the MPC algorithm. Second, errors resulting from the discretization procedure should be acceptable in order not to negatively affect the modeling accuracy, since the MPC performance is significantly affected by the accuracy of the discrete-time model. Choosing the appropriate discretization can be seen as a tradeoff between the first and second aspects, based on the application and control design requirements [23]. In this regard, the discretization methods are divided into three categories: exact, quasi-exact, and approximated methods [[22], ch. 7], [24], as shown in Fig. 4. The approximated methods are the most applied in power electronic

TABLE II
APPROXIMATED DISCRETIZATION METHODS

Method	Formulation
Forward-Euler	$\frac{d}{dt}x(t) = \frac{x(k+1)-x(k)}{T_s}$
Backward-Euler	$\frac{d}{dt}x(t) = \frac{x(k)-x(k-1)}{T_s}$
Bilinear (Tustin)	$\frac{d}{dt}x(t) = \frac{x(k+1)-x(k-1)}{2T_s}$

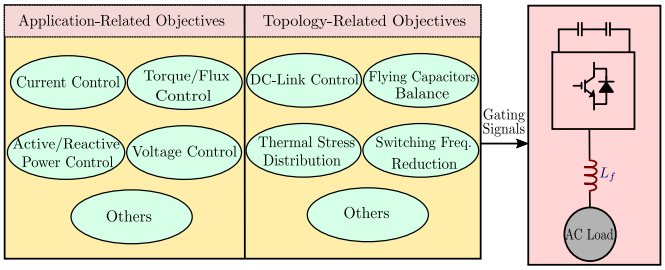

Fig. 5. Control objectives of MLI applications.

systems in general and MLI applications in particular due to their simplicity, straightforward implementation, and low calculation load [25], [26], [27], [28].

Forward-Euler, backward-Euler, and bilinear—also known as Tustin—approximations are three common methods that belong to the approximated family, as shown in Fig. 4. Table II shows the derivative approximation using these methods, where T_s is the sample period. By applying forward-Euler approximation to the system models in (6), (7), and (9), the predicted values $\mathbf{i}(k+1)$, $v_{fx}(k+1)$, and $\Delta v_c(k+1)$ are obtained as

$$\left.\begin{aligned}
\mathbf{i}(k+1) &= \left(1-\tfrac{R_f T_s}{L_f}\right)\mathbf{i}(k) + \tfrac{T_s}{L}(\mathbf{v}(k)-\mathbf{v}_g(k)) \\
v_{fx}(k+1) &= v_{fx}(k) + \tfrac{T_s}{C_{fx}}(s_{3x}-s_{4x})i_x \\
\Delta v_c(k+1) &= \Delta v_c(k) - \tfrac{T_s}{C}\sum_{x\in\{a,b,c\}}(s_{1x}s_{3x}+\bar{s}_{2x}\bar{s}_{3x})i_x
\end{aligned}\right\}. \tag{10}$$

B. Cost Function Formulation

The cost function formulates the MPC optimization problem including all control objectives, and thus, it defines the desired control behavior. The design of the cost function is a challenging task, especially in the multiple-objective problems typical in MLI applications. The issues related to the cost function such as formulation and norm, as well as the tuning of the WFs, are important research points because of their impact on the performance and stability of the whole system. The advances in addressing these issues in MLI applications are covered in Sections III-B and III-C.

The variables included in the cost function are determined by the MLI topology and the application under consideration. Accordingly, they can be divided into two groups: topology-related objectives and application-related objectives, as shown in Fig. 5.

Topology-related objectives are included to ensure proper operation of the MLI topology and mainly depend on the configuration of the inverter. For example, a dc-link balancing is a necessary objective for topologies with a mid-point clamped, such as NPC [13] and 5L-ANPC [29] inverters. Also, capacitor voltage control in FC-based topologies is an inevitable target, like FC [30] and 5L-ANPC inverters. In addition, thermal stress distribution among switches [31] and switching frequency reduction [13] are considered secondary objectives that can improve the converter operation and increase the power density and/or efficiency.

Application-related objectives are considered to meet the requirements of the load. For example, reference current tracking is a major goal in various applications such as in electric drives after generating the reference current according to the required machine speed/torque [32]. Also, torque and flux control are common objectives in drive systems [33]. Another example for application-related objectives is the active and reactive power control in grid-connected systems [34], [35], [36], [37] and voltage control in uninterruptible power supply (UPS) application [38].

For the considered case study in Fig. 3, the dc-link balancing and FC voltage control need to be included to ensure proper operation of the inverter. In addition, current control is considered as an application-related objective. By adopting the l_2-norm [39], the cost function g (also denoted as J) can be expressed as

$$\begin{aligned} g = {} & [\mathbf{i}^*(k+1) - \mathbf{i}(k+1)]^2 + \lambda_1[v^*_{fx}(k+1) - v_{fx}(k+1)]^2 \\ & + \lambda_2[\Delta v_c(k+1)]^2 \end{aligned} \tag{11}$$

where λ_1 and λ_2 are the WFs and used to adjust the priority among the control targets. WFs have a great influence on control behavior and stability. Thus, much research effort has been put into tuning or even eliminating WFs, as discussed in Section III-C. $\mathbf{i}^*(k+1)$ in (11) is the reference current at the $(k+1)$th sample and is determined by extrapolation methods. Extrapolation of reference variables is necessary to avoid the delay between the reference and the actual variable, especially when the sampling frequency is not significantly higher than the fundamental frequency. No extrapolation procedure is required in the steady-state operation when the MPC algorithm is designed in the dq-frame as the variables are dc values. However, when the references change, as in transient conditions, a delay arises, bringing the need for an extrapolation method. In this regard, three extrapolation methods are reported, namely, discrete-signal generator [22], vector angle extrapolation [22], [25], and Lagrange extrapolation [25], [34], [40]. The discrete-signal generator method is only used when the reference is determined by the user. The other two methods are used when the references are obtained from other control loops. In vector angle extrapolation, the variables must be in polar coordinate form ($re^{j\theta}$), and then, a discrete value $N_p\omega T_s$ is added to the angle θ to get the future value, where N_p and ω are the prediction horizon and variable angular frequency, respectively. Since this method is implemented in polar coordinates, it is only applicable to three-phase sinusoidal variables. Lagrange extrapolation is the most commonly used method in MPC because it can be used in single-phase systems and nonsinusoidal quantities. It uses the

TABLE III
SYSTEM PARAMETERS OF THE HIL IMPLEMENTATION

Parameter	Value
DC-link, V_{dc}	700 V
Grid voltage, $v_{g,l-l}$	380 V (rms)
Grid frequency, f_f	50 Hz
Filter resistance, R_f	0.1 Ω
Filter inductance, L_f	10 mH
DC-link capacitors, C_1 and C_2	2000 μF
FC, C_f	1000 μF
Sampling time, T_s	100 μs

present and past samples to predict the future value without involving any phase angle calculations. The number of past samples defines the order of the extrapolation [41]. Adopting a third-order Lagrange extrapolation, $\mathbf{i}^*(k+1)$ in (11) is obtained as

$$\mathbf{i}^*(k+1) = 4\mathbf{i}^*(k) - 6\mathbf{i}^*(k-1) + 4\mathbf{i}^*(k-2) - \mathbf{i}^*(k-3). \tag{12}$$

C. Optimal Vector Identification Through the Optimization Algorithm

Once the discrete-time model is constructed and the optimization problem is formulated via a cost function, an optimization algorithm is applied to identify the optimal control action. Typically, an exhaustive search algorithm (ESA) is used to solve the optimization problem by checking all the converter states to find the optimal one. However, in MLI applications, the large number of states leads to a heavy computational burden, resulting in a long sampling period to be used as the optimization problem is solved online. On the other side, in power converter applications, the sample period tends to be short, on the order of tens of microseconds, for high control performance. Accordingly, much effort has been focused on investigating other optimization algorithms, as discussed in Section III-A. With long-horizon FCS-MPC, this issue is more apparent, and hence, other optimization algorithms are used such as sphere decoding algorithm (SDA) [42]. More details about the implementation of long-horizon MPC are provided in Section III-E.

For the 5L-ANPC inverter, each phase has eight switching states, as shown in Table I, which means 512 (8^3) states in the three-phase implementation. With the conventional FCS-MPC concept using ESA and a horizon of one, it is required to carry out 512× predictions for the controlled variables according to (10) and 512× cost function evaluation according to (11) per each control sampling period T_s. Note that the number of calculations increases exponentially as the number of prediction steps N_p increases.

The implementation of the conventional FCS-MPC for the case study considered in Fig. 3 is verified by a hardware-in-the-loop (HIL) implementation. The system parameters are given in Table III. Fig. 6 shows the HIL results for a step change in the reference current from 10 to 5 A. As it is clear, the three control objectives considered in the cost function are well achieved. The grid currents follow the reference with high dynamic performance. The FCs C_{fa}, C_{fb}, and C_{fc} are stabilized at its reference $V_{dc}/4 = 175$ V. In addition, the voltages of the dc-link capacitors are well balanced.

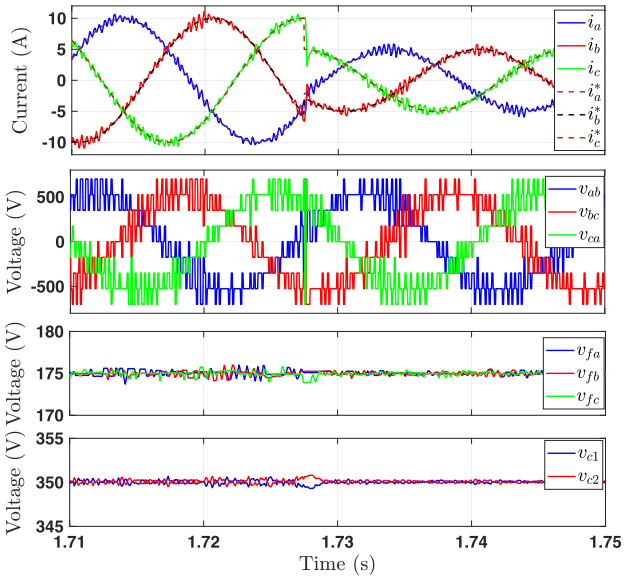

Fig. 6. HIL results of standard FCS-MPC.

An analysis of recent advances related to FCS-MPC for MLIs reveals that the published papers aim to address one or more of the following issues:

1) computational burden reduction;
2) cost function design;
3) WFs design or elimination;
4) fixed-switching-frequency operation;
5) long-horizon MPC.

The advances and improvements related to these issues are discussed in the following section. Model uncertainty and observer design are common issues shared by all the MPC methods, so these are addressed in Section VI for the direct and indirect MPC methods.

III. FCS-MPC: CHALLENGES AND RECENT ADVANCES

A. Computational Burden Reduction

In FCS-MPC, the optimization problem needs to be solved online. In the case of MLIs in particular, this leads to a high computational load due to the large number of converter states, necessitating the use of a long sampling period, which is undesirable in power electronics applications. Several solutions have been presented to reduce the computational load to realize a successful practical implementation using the standard digital platforms.

Many works have been proposed to reduce the complexity of FCS-MPC for three-phase MLIs. The first attempt was reported in [43] for the 5L-CHB inverter. In this article, the reduction of the computational load is realized in two steps: 1) by eliminating the redundant states that produce high CMVs, reducing converter states from 125 to 61 switching states and 2) assuming that the optimal voltage vector is adjacent to that previously applied, only seven vectors are evaluated in each sample. Accordingly, for each different vector, a list of the closest seven vectors is defined

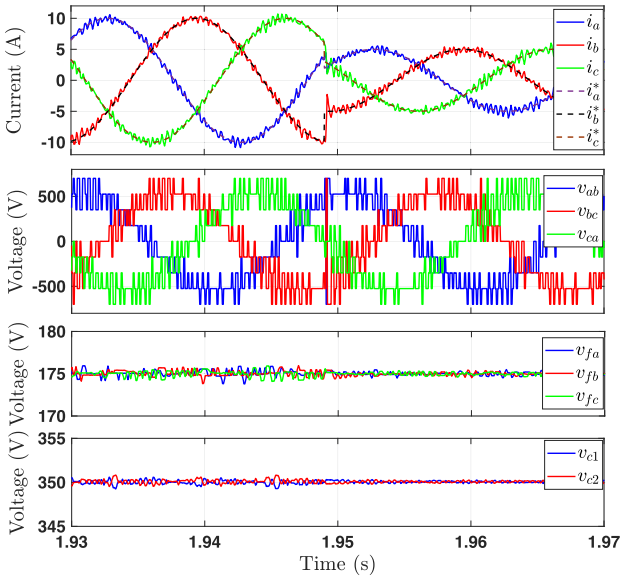

Fig. 7. HIL results of voltage-vector-based FCS-MPC.

offline and stored in a database. Despite the reduction of the online calculations and acceptable steady-state performance, this method suffers from poor dynamic performance and requires significant memory space to store the lookup tables (LUTs).

An interesting approach was presented in [44], where the current control objective is represented by the converter voltage in the cost function. For illustration, the cost function in (11) is rewritten as

$$g = [\mathbf{v}^*(k) - \mathbf{v}(k)]^2 + \lambda_1[v^*_{fx}(k+1) - v_{fx}(k+1)]^2 + \lambda_2[\Delta v_c(k+1)]^2 \tag{13}$$

where the reference voltage $\mathbf{v}^*(k)$ is calculated from the system model using the deadbeat concept. Taking the grid-connected system in Fig. 3 as an example, $\mathbf{v}^*(k)$ is obtained as

$$\mathbf{v}^*(k) = R_f\mathbf{i}(k) + L_f\frac{\mathbf{i}^*(k+1) - \mathbf{i}(k)}{T_s} + \mathbf{v}_g(k). \tag{14}$$

This method replaces the computational burden of current predictions with only one voltage reference estimation; hence, it is called single-predictive FCS-MPC. Considering the 5L-ANPC inverter, the single-predictive FCS-MPC saves 512× current predictions by estimating $\mathbf{v}^*(k)$ according to (14) only once per sample. However, the predictions of the other variables (e.g., FCs and dc-link voltages) are still required for all the converter states. This concept has been the basis for several developed low-complexity FCS-MPC methods. These FCS-MPC methods that are based on reference voltage estimation are also referred to as voltage-based FCS-MPC because the cost function is expressed by a voltage as given in (13) rather than the current in the traditional method [45]. The HIL results of the voltage-based FCS-MPC for the grid-connected 5L-ANPC converter are shown in Fig. 7. The implementation is carried out with the same system parameters in Table III. As can be observed, the results are very similar to those of the standard FCS-MPC in Fig. 6, demonstrating the ability of the voltage-based FCS-MPC to identify the optimal state as in the standard method.

The computing effort has been further reduced in [44] by dividing the space vector (SV) diagram into six sectors and only evaluating the vectors of one sector based on the reference voltage location. In [45], the SV diagram of the 5L-CHB inverter is divided into 96 triangle regions. After calculating $\mathbf{v}^*$, one triangle is located based on the magnitude and angle of $\mathbf{v}^*$. Although the evaluated vectors are reduced to three, many calculations are performed offline and stored in LUTs, which requires a large storage space. Yang et al. [46] reduced the number of evaluated vectors from 27 to only 3 for the three-level (3L) T-type inverter by dividing the SV diagram into 24 triangular regions. Moreover, dc-link balancing is realized by exploiting the redundant states without the need for capacitor voltage predictions or WFs. However, determining the appropriate triangle is not an easy task and requires storage for LUTs. An S-algorithm is proposed in [47] to locate the closest vector to the reference voltage for the 3L-NPC converter. In this method, three imaginary axes denoted as S_1, S_2, and S_3 are added to the SV diagram, and the coordinates of the reference voltage with respect to these axes are determined using analytical formulations. Once the reference voltage positions are identified, the optimal vector can be located. The S-algorithm can be applied to higher level topologies. However, the other control objectives, such as dc-link and FC balancing, can only be achieved using the redundant states, which is a limitation for MLI topologies with an insufficient number of redundant states. Voltage-based FCS-MPC has been the basis for other developed computationally efficient algorithms for various MLI topologies [48], [49], [50], [51], [52]. Another reduction concept of the FCS-MPC for three-phase MLIs is reported in [53]. The idea of this work is to neglect the correlation between the control objectives of the three phases. Considering the system model in (3), the CMV is assumed to be zero $V_{nN} = 0$, resulting in

$$v_{xN} \approx R_f i_x + L_f\frac{d}{dt}i_x + v_{gx}. \tag{15}$$

With this approximation, the variables of each phase are controlled independently, reducing the total number of converter states from N_{st}^3 to $3 \times N_{st}$, where N_{st} is the number of switching states of the single-phase leg. However, all the redundant states resulting from the correlation of the three phases are ignored, which negatively affects the control performance. Applying this model-approximated FCS-MPC to the 5L-ANPC in Fig. 3, the number of evaluated converter states is reduced from 512 to 24. The results of the approximated-model FCS-MPC are depicted in Fig. 8. Despite the reduction in computation, the control performance has been degraded compared to the standard FCS-MPC in Fig. 6. Lower tracking quality and higher voltage ripples in the FCs and dc link are observed in this method. This is due to the approximation in the system model, which led to ignoring the redundancies of the three-phase converter.

To compare the calculation load, six prior-art methods are implemented on dSPACE Microlabbox for the grid-connected 5L-ANPC converter. The implemented methods are the conventional scheme, single-predictive and six-sector FCS-MPC methods presented in [44], computationally efficient FCS-MPC presented in [45], S-algorithm method reported in [47], and

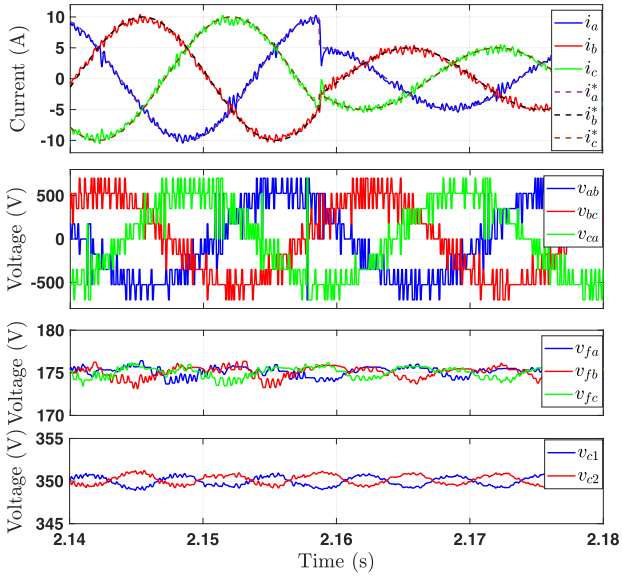

Fig. 8. HIL results of approximated-model-based FCS-MPC.

TABLE IV
EXECUTION TIME OF REDUCED COMPUTATIONAL BURDEN FCS-MPC SCHEMES ON DSPACE MICROLABBOX

Method	MPC Algorithm	Total Time
Conventional FCS-MPC	16 µs	35 µs
Single-predictive FCS-MPC	14.5 µs	33.4 µs
Six-sector FCS-MPC	4.12 µs	23 µs
Computationally efficient FCS-MPC	1.22 µs	20.2 µs
S-Algorithm FCS-MPC	1.15 µs	20.14 µs
Model-approximated FCS-MPC	1.08 µs	20 µs

model-approximated FCS-MPC proposed in [53]. The execution times are measured from ControlDesk software using a *turnaround* variable. Table IV lists the execution times required for the implemented methods, demonstrating the feasibility of computation reduction .

For the single-phase MLIs, only few works have been presented in the literature. In [54], the computational effort of the single-phase 3L-NPC converter has been reduced by avoiding the cost function evaluation. However, in contrast to the standard FCS-MPC, complex analyzes are performed to solve the optimization issue. In addition, NP balancing is not included in the MPC method; thus, a proportional–integral–derivative controller is utilized, which complicates the overall control and inserts the issue of proportional–integral (PI) tuning. A computationally efficient FCS-MPC for a four-level (4L) hybrid H-bridge MLI is presented in [14]. In this approach, only 16 states are evaluated instead of 64 vectors of the standard MPC. However, neglecting 48 states caused the MLI to lose one of its features, the high number of redundancies, that can be exploited to realize better FC balance or to minimize the switching frequency. In addition, owing to redundancy elimination, two power switches do not carry current with this MPC method, which adversely affects the loss sharing between the power devices. In [55], low-complexity voltage-based FCS-MPC is reported for the nine-level ANPC-based inverter. In this method, the converter states are divided into two sets and only one set is considered in the optimization process based on the calculated reference voltage. Moreover, the prediction of the dc-link voltages is avoided by integrating the NP control into the FC balance objective. Other computationally efficient FCS-MPC methods have been proposed for single-phase MLIs in [15], [56], [57], and [58].

B. Cost Function Design

One of the biggest advantages of the FCS-MPC algorithm is that multiple control targets and constraints can easily be included in a single cost function. A cost function is used to evaluate the predictions of the system variables and is usually structured as a sum of errors of the controlled variables. In power electronics control applications, it typically contains a tracking error (primary objective) and control effort penalization (secondary objective)

$$J(y(k),u(k)) = \| y_{\text{ref}}(k+1) - y(k+1)^P \|_l^l + \| \lambda_u \Delta u(k) \|_l^l \tag{16}$$

where $y_{\text{ref}}(k+1)$ is the reference value and $y(k+1)^P$ is the predicted value, λ_u is the WF, which adjusts the tradeoff between the control objectives, and $\Delta u(k)$ defines the switching effort. Which control variables will be included in the cost function depends on the converter topology and application. The choice of the norm (l) also has a high impact on the performance of the designed FCS-MPC algorithm [39], [59]. The l_1-norm for an n-dimensional vector y_n is defined as a sum of absolute values, while for l_2-norm, it is defined as a sum of square values

$$\| y \|_1 = |y_1| + |y_2| + \cdots + |y_n| \tag{17}$$

$$\| y \|_2 = y_1^2 + y_2^2 + \cdots + y_n^2. \tag{18}$$

In terms of the computation effort, the l_1-norm is lighter due to a lower number of calculations; however, the analysis conducted in [39] revealed that the use of l_1-norm can result in a performance deterioration and closed-loop instability if $\lambda_u \neq 0$. There exist a critical value $\lambda_{u,\text{crt}}$, for which, if the penalty of switching exceeds this value, the controller will not be able to switch. This limits the switching frequency range significantly. Therefore, the MPC algorithm with l_1-norm will not be able to keep the stability at low switching frequency operation, which are typically required for high-power high-voltage motor drives—one of the main application areas of the MLI topologies. Further analysis also showed that l_2-norm of a ripple variable is proportional to the total harmonic distortion (THD); thus, by minimizing the l_2-norm of the output ripple ($y_{\text{ref}} - y^P$), better performance is achieved than for l_1-norm. Since the l_2 -norm transforms the optimization problem into a quadratic problem, the solution to the unconstrained problem can be obtained by setting the derivative of the cost function to 0. This feature enables the use of both FCS-MPC with implicit modulator and indirect MPC [24]. Thus, the use of l_2-norm is recommended to ensure the closed-loop stability of the system, wide range switching frequency operation, and low distortion.

Cost function structures used in FCS-MPC applications for MLIs have at least two control targets in the cost function. Exceptions are sequential [60], [61] and cascaded MPC algorithms [48], which use separate cost functions for each control targets

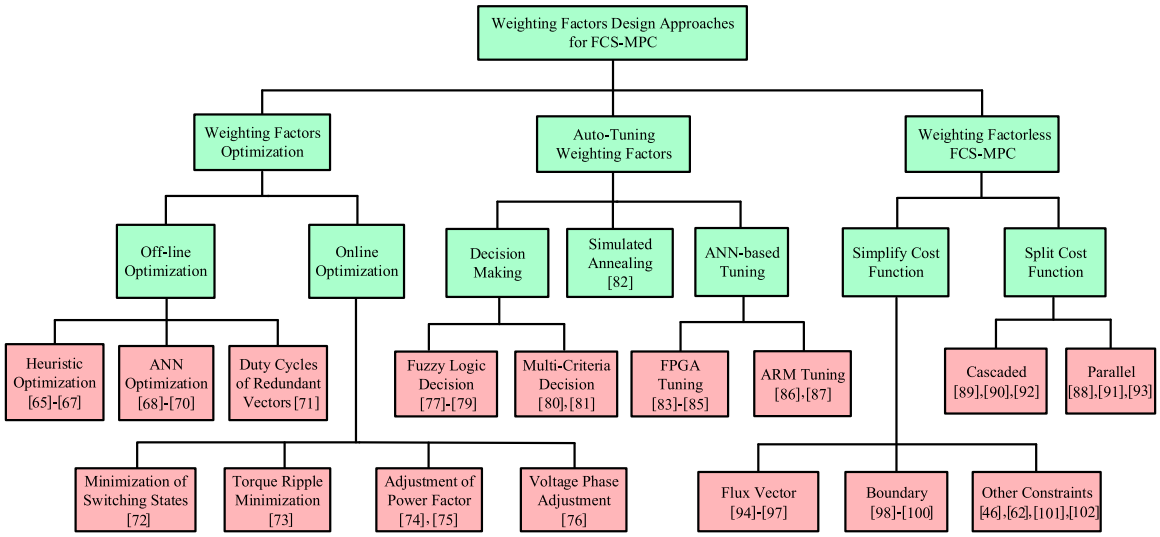

Fig. 9. Classification of WF design for FCS-MPC.

and FCS-MPC algorithms, which use another control method or LUTs to control the secondary objective like, e.g., NP voltage in NPC converters or CMV [26], [62].

A problem specific to some MLI topologies is uneven device loss distribution. This problem becomes even more apparent when in one converter topology, Si devices are combined with wide-bandgap devices like SiC diodes or MOSFETs to increase the conversion efficiency. For both performance and reliability, this is a limiting factor since the hottest device will define the maximum transferable power. Moreover, the device, which is set under the largest thermal stress, will have a much faster wear-out, leading to lower lifetime. Since the FCS-MPC is typically not using a modulator, it is very simple to impose restrictions on the certain switching commutation or reduce the switching frequency using the cost function design. For example, in [63], a hybrid Si/SiC 3L-NPC is using the cost function (19), which takes into account the reduced switching losses in the commutations involving the SiC diodes to achieve lower overall losses without neglecting the output current tracking error

$$J = |i^*(k) - \hat{i}(k+1)| + c_{\text{sw}} \tag{19}$$

$$c_{sw} = \begin{cases} 0, & \text{no switching event} \\ k, & \text{no SiC diode used} \\ k \cdot k_1, & \text{a SiC diode used} \end{cases} \tag{20}$$

where k and k_1 are tunable and define the penalty. Another example is given in [64] for the 3L-NPC converter, where control actions that switch devices during the period of high current amplitude are penalized in order to reduce the switching losses

$$J = |I_a(k)| \cdot n_a + |I_b(k)| \cdot n_b + |I_c(k)| \cdot n_c \tag{21}$$

$$n_x = |u_{x1}(k) - u_{x1}(k-1)| + |u'_{x2}(k) - u'_{x2}(k-1)| \tag{22}$$

where $I_x(k)$ is the amplitude of phase x of the converter output current, $u_{x1}(k)$ and $u_{x1}(k-1)$ are the current and previous switching states of the outer devices, respectively, and $u'_{x2}(k)$ and $u'_{x2}(k-1)$ are the current and previous switching states of the inner devices, respectively.

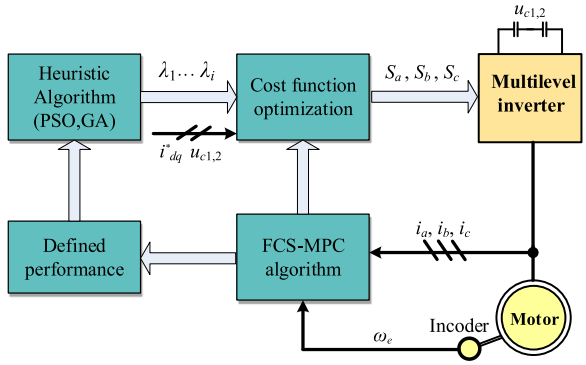

Fig. 10. Concept of heuristic algorithm for optimizing WFs.

C. WF Design or Elimination

WFs directly influence the system control performance, especially for MLIs, where there are multiple control targets [65]. Therefore, it is mandatory to optimize the cost function and optimally tune the WFs. A lot of solutions have been proposed for designing WFs, which can be classified into three categories, as shown in Fig. 9.

1) WF Optimization: The optimization of WFs is a very challenging task for cost functions with multiple objectives that are in conflict or cannot be unified. Several approaches have been proposed for tuning the WFs of FCS-MPC, including offline optimization [65], [66], [67], [68], [69], [70], [71] and online optimization [72], [73], [74], [75], [76].

The offline optimization mainly utilizes the heuristic algorithm [65], [66], [67] and artificial neural network (ANN) [68], [69], [70] to search the global optimal WFs for the cost function of FCS-MPC. The concept of heuristic method for searching the optimal WFs of FCS-MPC is presented in Fig. 10. The heuristic methods, such as genetic algorithm (GA) [65], [66] and particle swarm optimization (PSO) [67], are employed to find the optimal combination of WFs ($\lambda_1 \cdots \lambda_i$), according to the predefined performance. The heuristic optimization can

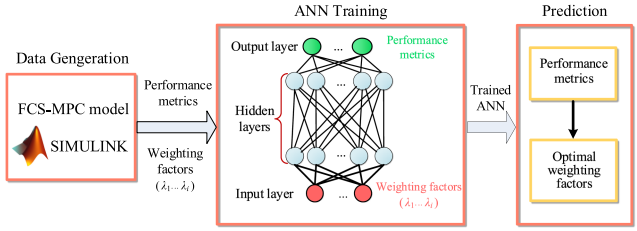

Fig. 11. Block diagram of ANN optimization for the WFs.

accurately find the optimal WFs of FCS-MPC for achieving the defined performance. As for ANN-based optimization, Fig. 11 depicts the block diagram of ANN optimization for the WFs. In Fig. 11, the ANN-based method first generates the dataset from simulations. Then, the dataset is classified into the training set and the validation set to train and evaluate the ANN. After the ANN is trained, it is applied to predict the WFs according to the corresponding performance metrics. Another offline optimization of WFs is to reduce the terms of cost functions so as to reduce the time effort to search the optimum WFs of FCS-MPC. In [71], the voltage vector is selected to minimize the primary objectives, and then, the duty cycle of redundant vectors is employed to control the secondary objectives. Consequently, the cost function of FCS-MPC does not include the terms of NP voltage balancing.

In summary, the offline optimization of WFs neither imposes the computation burden nor deteriorates the dynamic performance of FCS-MPC. However, those approaches fail to be robust to the system parameter mismatch, and the WFs should be manually adjusted instead of automatically tuning.

The online optimization enables the cost functions to perform an automatic adjustment of WFs, and it is adaptive to time-varying working conditions. The online optimization methods mainly concentrate on designing an observer function used to monitor the performance of FCS-MPC, and then, the designed observer minimizes the cost function by adjusting switching states [72], torque ripple [73], power factor [74], [75], and voltage phase [76].

In [72], a new observer function was proposed, which quantifies the contribution of each switching state to eliminate the existing error, instead of considering the total error value. The optimization in [73] is based on dividing the control interval into two parts: active time for applying the active voltage vectors and zero time for applying the zero voltage vector. With this technique, the torque ripple is calculated as a function of WF. The WF optimization in [74] and [75] is realized by predicting the absolute tracking errors of the control objectives and corresponding constraints, where the active power and reactive power are regulated and the power control can be bidirectionally decoupled. The observer function in [76] is formulated with four constraints (torque, stator flux, CMV, and switching losses), and this method regulates the voltage phase to minimize the observer function to improve both steady-state and dynamic performance.

The online optimization achieves the automatic adjustment of WFs to improve the performance of FCS-MPC. However, the online optimization methods increase the computational burden and complicate the controlling procedure of FCS-MPC.

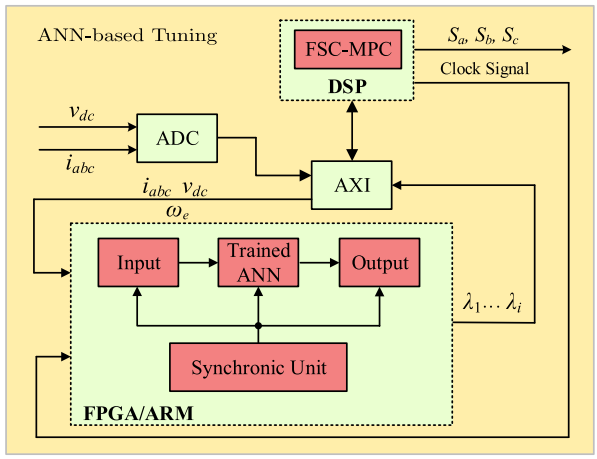

Fig. 12. Procedure of ANN-based tuning of WFs.

It should be mentioned that the abovementioned optimization approaches strongly depend on system parameters, and most of them were designed for two control objectives. When more objectives are considered, especially for MLIs, the WFs can be obtained using trial-and-error procedures.

2) Autotuning WFs: With respect to the autoturning of WFs, it is mainly realized by decision making [77], [78], [79], [80], [81], simulated annealing [82], and ANN-based tuning [83], [84], [85], [86], [87].

Both the fuzzy logic decision making [78], [79] and multicriteria decision [80], [81] can be employed to replace the standard selection stage of the cost function. As a result, the WF selection is avoided, and a simple selection scheme is obtained. The fuzzy logic decision making is designed to be the switching state selector for FCS-MPC in induction motor drives [77], [79] and direct matrix converter [78]. Besides, the fuzzy logic decision making can promote the design of the FCS-MPC state selector to be feasible for MLIs. It should be noted that the switching selectors of FCS-MPC can also be replaced by multicriteria decision-making methods named TOPSIS [80] and VIKOR [81]. The decision making avoids the WF selection, and it is much suitable for MLI systems. Nevertheless, it increases the computation demand and fails to tackle the problem of preference absence among the criteria of decision making.

With the help of field-programmable gate array (FPGA) and advanced RISC machines (ARMs), the autotuning of WFs for FCS-MPC can be achieved by intelligent algorithms. The intelligent algorithm simulated annealing [82] is implemented into an FPGA and searches the optimal combination of WFs to minimize the cost functions. The process of ANN-based autoturning is presented in Fig. 12. The information of sensors ($V_{\rm dc}$, i_{abc}, and ω_e) is transmitted into the input layer of the trained ANN in FPGA/ARM, where the ANN is trained by simulation data. Then, the ANN outputs the WFs for FCS-MPC, and the clock signal is transmitted into the synchronic unit to update the trained ANN, where the AXI is the agreement of control bus. Through the ANN-based tuning of WFs, FCS-MPC achieved the robust controlling for a dc–dc boost converter [83], low switching frequency for modular multilevel converter [84],

constant switching of better dynamical response for 2L voltage-source inverters [85], better dynamic response for the 3L-NPC inverter [86], and better reliability for seven-level (7L) modified packed U-cell active rectifier [87].

In conclusion, the autotuning of WFs via intelligent algorithm not only avoids the WF selection but also enhances the control performance of FCS-MPC. It should be mentioned that the performance of intelligent algorithm is limited to the logic resources of FPGA/ARM.

The autotuning approaches can realize the dynamic adjustment of WFs for FCS-MPC. Although the artificial-intelligence-based tuning effectively promotes FCS-MPC to be robust to the mismatch of system parameters, the cost and logic resources of the microcontrollers (e.g., FPGA and ARM) should be taken into consideration in the industrial applications.

3) Weighting Factorless FCS-MPC: Since the tuning of WFs is quite cumbersome, the weighting factorless MPC becomes a very attractive solution. The reported methods to avoid the use of WFs can be roughly categorized as split the cost function and simplify the cost function.

Split the cost function is quite intuitive and easy for implementation, where the control objectives are optimized with independent cost functions. Split the cost function is frequently adopted for predictive torque control to eliminate the flux weights, as seen in [88], [89], [90], and [91]. The cost function for torque and flux magnitude was processed in sequential or by parallel. However, this method may lead the algorithm to be even complex, and it should take care that improper design will deteriorate the performance compared to the FCS-MPC with original cost function [59]. In [92], a cascaded MPC method was proposed for 3L-ANPC inverter drives. In this method, the reference tracking, NP potential balance, and the loss distribution were achieved in sequential, and each stage adopts an independent cost function without WF.

The utilization of a split cost function can also be observed in [93] for grid-connected seven-level packed U-cell (PUC7) inverters. Inspired by sliding-mode control theory, this controller employs two parallel cost functions: one for FC control and the other for current tracking. The design has low average switching frequency by incorporating an additional parameter to control the FC within a hysteresis band.

Simplify the cost function usually adopts the extra constraints based on the specific optimization targets to reduce the terms. For predictive torque control, the most common way is to convert the tracking for torque and flux magnitude into the stator flux vector tracking, which can be quite similar to the predictive current control [94], [95], [96], [97]. To achieve the multiple control objectives without WFs, the boundary-based method can be a very effective way. In [98] and [99], the trajectories of torque, flux magnitude, and NP potential are extrapolated with a set of input sequences. The candidate voltage vector sequences can maintain three control objectives within their boundaries for the given prediction horizon, separately. Then, the cost function only needs to penalize the commutation times, and the sequence with the lowest switch transition is selected. Thus, the low-switching-frequency operation can be achieved simultaneously. In [100], a boundary with current error extrapolation was presented, where the cost function selected the voltage vector that achieves the longest duration time within the boundary. However, the computational burden with long-horizon prediction could be a challenge. Another example of simplifying the cost function can be seen in [101] and [102] for the application of the PUC7 grid-connected inverter, as detailed in Section IV.

In [46], the LUT method was adopted to achieve the NP potential balance, where the complementary small voltage vectors were assigned to the two predefined tables. Depending on the state of the NP potential, one of the tables is chosen for prediction. A similar method was reported in [62], while the CMV reduction was also considered in the LUT.

D. Fixed-Switching-Frequency MPC

One of the main features of FCS-MPC is that it does not use a modulator to generate the switching pulses for MLIs. This results in a high dynamic performance on the one side and a degraded performance in steady-state compared to pulsewidth modulation (PWM)-based methods. Because in FCS-MPC, only one vector is applied during the whole control period T_s, producing higher ripples in the waveform. Due to the variable switching frequency, FCS-MPC produces a wide harmonic spectrum [103] and, as a result, complicates the filter design.

An early solution to the variable switching frequency issue is the hybrid FCS-MPC [104]. This technique uses a low-pass filter as a demodulation stage after the standard FCS-MPC to remove the high-frequency components, as shown in Fig. 13(a). Then, the output of the low-pass filter is modulated by a sinusoidal PWM or space vector modulation stage. This approach is intuitive and practical and does not increase the computational load. However, the dynamic and steady-state performance is degraded compared to the standard FCS-MPC. In addition, it necessitates the use of an external modulator.

Another effective approach for this matter is the modulated MPC (M2PC) [17] [see Fig. 13(b)]. This method simulates the behavior of the PWM technique by introducing the concept of variable switching time and applying two vectors (or more) during the control cycle T_s. The implementation of the M2PC for MLIs was first presented in [17] for a 7L-CHB converter. The duration times of the vectors are determined to be inversely proportional to their corresponding cost function values. In other work, the duration times are calculated using a partial derivative to minimize the total cost function of the selected vectors [105]. M2PC has been applied to different MLI topologies in different applications, such as NPC converter in grid-connected applications [106] and CHB converter in STATCOM [107]. Another method is the model-predictive pulse pattern control. This method is used to reduce harmonic distortion or remove specified harmonics, which are calculated offline at that instant of time [8], [108].

Optimal switching sequence MPC (OSS-MPC) is another efficient fixed-switching-frequency technique that was first applied to MLIs in [109] for a grid-connected NPC converter. The concept of approach is to divide the converter states into a limited number of sequences (Seq_1 to Seq_n). The optimal sequence (Seq_{opt}) is identified by optimizing the cost function

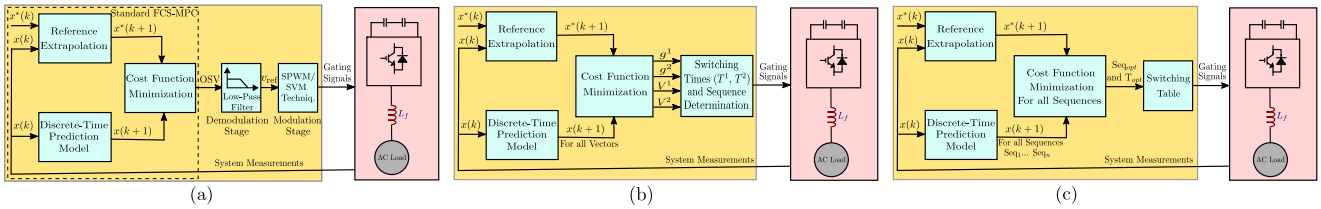

Fig. 13. Most common FCS-MPC methods with fixed switching frequency. (a) Hybrid FCS-MPC. (b) Modulated MPC. (c) Optimal switching sequence MPC.

for all the sequences, as shown in Fig. 13(c). This method has a better steady-state performance with an improved harmonic spectrum compared to conventional FCS-MPC. However, the computational effort is higher, and the design of the switching sequences is a challenging task for MLIs, especially for three-phase implementation. The application of this method with an NP potential control as a second control target for a full-bridge NPC converter is presented in [54] and [110]. A similar method is reported in [111] for a T-type converter by applying three vectors per control cycle. In addition, NP potential control is achieved exploiting the converter redundancies, eliminating the use of a WF. However, the cost function is formulated with the estimated voltage, increasing control sensitivity to model parameters.

E. Long-Horizon FCS-MPC

Owing to the direct manipulation of the switch positions of the power converter $\boldsymbol{u} = [u_a \ u_b \ u_c]^T \in \boldsymbol{\mathcal{U}} \subset \mathbb{Z}^3$ (with N_{st} defining the size of the integer input set), the formulation of the optimization problem underlying FCS-MPC denotes an *integer optimization problem* also called integer program.[1] The latter is inherently difficult to solve as it is known to be *NP*-hard, i.e., the computational complexity (and solution time) increases exponentially with the number of candidate switching sequences to be evaluated in the optimization problem [59], [112]. Therefore, the practical realization of real-time implementation of FCS-MPC with long prediction horizons is not trivial [24].

Consider the sequence of manipulated variables over a prediction horizon of $N_p \in \mathbb{N}^+$ time steps

$$\boldsymbol{U}(k) = \left[\boldsymbol{u}^T(k) \ \boldsymbol{u}^T(k+1) \ \ldots \ \boldsymbol{u}^T(k+N_p-1)\right] \in \mathbb{U} \tag{23}$$

where $\mathbb{U} = \boldsymbol{\mathcal{U}}^{N_p}$ is the feasible set, which grows exponentially with the number of horizon steps. For long-horizon FCS-MPC, the control objectives (e.g., current and/or voltage reference tracking) are quantified by a (generalized) objective function $J \to \mathbb{R}^+$ of the form

$$J\left(\boldsymbol{x}(k), \boldsymbol{U}(k)\right) = \sum_{\ell=k}^{k+N_p-1} \Lambda\left(\boldsymbol{x}(\ell+1), \boldsymbol{u}(\ell)\right) \tag{24}$$

where $\boldsymbol{x}$ is the state of the system and $\Lambda(\star)$ is the stage cost based on the p-norm, i.e., (24) may resemble (11) and (16). In the case of MLIs, by adopting a short prediction horizon—e.g., $N_p = 1, 2$—and reducing the size of the feasible set $\mathbb{U}$ with the methods

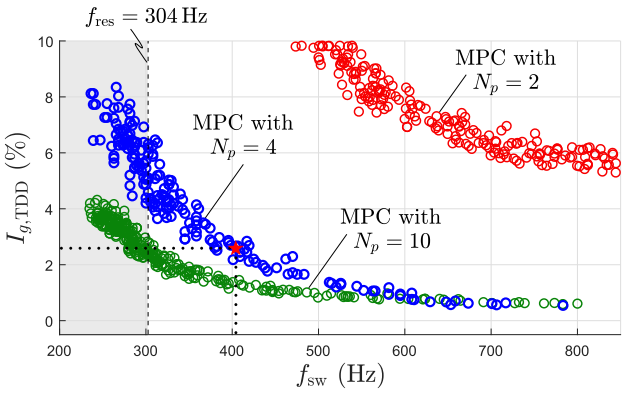

Fig. 14. Tradeoff between grid current TDD $I_{g,\text{TDD}}$ and switching frequency f_{sw} for FCS- MPC with $N_p = 2$ (red circles), $N_p = 4$ (blue circles), and $N_p = 10$ (green circles). Each data point (round circles) corresponds to a steady-state simulation. Note that, for the considered third-order system (3L-NPC converter with an LCL filter), the state vector consists of the converter current $\boldsymbol{i}_{\text{conv},\alpha\beta}$, capacitor voltage $\boldsymbol{v}_{c,\alpha\beta}$, grid current $\boldsymbol{i}_{g,\alpha\beta}$, and grid voltage $\boldsymbol{v}_{g,\alpha\beta}$, i.e., $\boldsymbol{x} = [\boldsymbol{i}^T_{\text{conv},\alpha\beta} \ \boldsymbol{v}^T_{c,\alpha\beta} \ \boldsymbol{i}^T_{g,\alpha\beta} \ \boldsymbol{v}^T_{g,\alpha\beta}]^T$, while the output vector is $\boldsymbol{y} = [\boldsymbol{i}^T_{\text{conv},\alpha\beta} \ \boldsymbol{v}^T_{c,\alpha\beta} \ \boldsymbol{i}^T_{g,\alpha\beta}]^T$, i.e., multiple current/voltage control. The sampling interval is $T_s = 150\mu$s. See [120].

detailed in Section III-A, the FCS-MPC problem can be solved online in a straightforward and numerically feasible manner with exhaustive enumeration (keeping the computational complexity at bay) [113]. This relates to the formulation derived in Sections II and III. However, it has been proven that employing FCS-MPC with long prediction horizons can significantly reduce the total demand distortion (TDD)—e.g., current TDD, I_{TDD}—and notable improvements under steady-state operating conditions can be achieved [114], [115].

1) Benefits: In particular, when MLIs are the targeted applications, long horizons strongly impact the closed-loop performance [116], [117], [118]. Such higher order systems[2] are subject to more complex dynamics. A long prediction horizon enables the controller to make better educated decisions because the evolution of the system state is computed over a longer time interval into the future. This performance boost is visible in Fig. 14. A third-order system is considered, namely an MV grid-tied 3L-NPC converter with an LCL filter and a resonance frequency $f_{\text{res}} \approx 304$ Hz. The corresponding scheme, system parameters, and full derivation of the optimization problem are summarized in [120] and [121]. Extending the prediction

[1]Note that, if the objective function $J(k)$ is quadratic, the problem relates to an integer QP (IQP).

[2]For instance, complex converter topologies (series/parallel, modular) [119] with coupled inductors and LC or LCL filters.

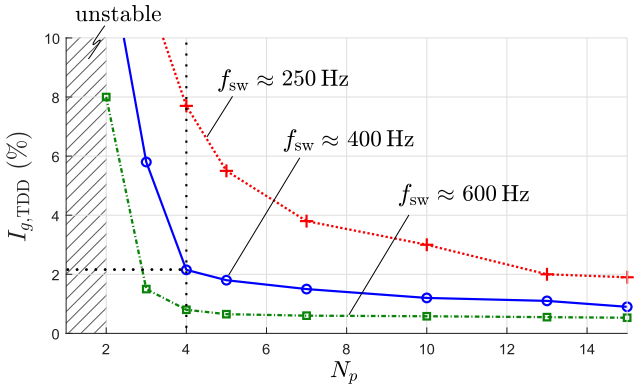

Fig. 15. Grid current TDD $I_{g,\mathrm{TDD}}$ as a function of the prediction horizon N_p at different switching frequencies. Individual simulations are shown as "sum," "square," and "circles," respectively. See [120].

horizon from two to ten steps reduces $I_{g,\mathrm{TDD}}$ by more than 9% at a switching frequency $f_{\mathrm{sw}} = 400$ Hz. Similar benefits hold over the whole frequency range. Moreover, the proposed MPC algorithm can operate the converter at significantly lower switching frequencies close or below f_{res}. This is only possible with a sufficiently long prediction horizon, while, on the contrary, $N_p = 2$ is clearly not suitable for industrial applications where grid standards—e.g., IEEE 519 and IEC 61000-2-4—are concerned.

This can also be observed in Fig. 15, which depicts the grid current TDD as a function of the prediction horizon length N_p for a fixed set of switching frequencies. The current THD decreases considerably up to the ten-step horizon, after which the rate is significantly lower. Note that a one-step horizon leads to an unstable behavior for such system.

Combining Figs. 14 and 15, the *proverbial knee* of the fitted curves given by $N_p = 4$ and $f_{\mathrm{sw}} = 400$ Hz indicates a good tradeoff between performance (i.e., $I_{g,\mathrm{TDD}}$) and controller complexity (i.e., size of $\boldsymbol{U}$ and choice of T_s). Nevertheless, $\boldsymbol{U} \in \boldsymbol{\mathcal{U}}^4$ switching sequence has to be evaluated in the optimization problem to find the optimal sequence $\boldsymbol{U}^*$ within the sampling interval T_s. Adopting an exhaustive enumeration criterion is computationally unfeasible when considering real-time implementation onto industrial embedded hardware [24].

2) Methods: To reduce the computational load without sacrificing the optimality of the solution, methods that rely on dedicated optimization algorithms, such as branch-and-bound [42], and nontrivial prediction horizon formulations, such as move blocking strategies [112], event-based horizons [8], and prediction with extrapolation or interpolation [99], [122], [123], [124], should be considered.

a) Sphere decoding algorithm: In case the optimization problem underlying FCS-MPC is based on a linear prediction model subject to linear *hard* constraints, the branch-and-bound algorithms named *sphere decoder* can be efficiently employed [42]. Applying the sphere decoder requires the reformulation of the underlying optimization problem into an integer least-squares (ILS) one. By doing so, the search for the optimal solution $\boldsymbol{U}^*$ can be written in terms of the unconstrained solution, i.e., the solution that minimizes (24) when relaxing the feasible set from $\mathbb{U}$ to $\mathbb{R}^{3N_p}$. The optimal integer solution relates to the lattice point with the shortest Euclidean distance to $\boldsymbol{U}_{\mathrm{unc}}$. In the next step, a $3N_p$-dimensional hypersphere of radius ρ centered at the unconstrained solution $\boldsymbol{U}_{\mathrm{unc}}$ is computed. By doing so, only the candidate solutions inside the sphere have to be evaluated. The goal of the optimizer is to tighten the radius ρ incrementally until only the optimal solution remains inside the sphere, whereas all other candidate solutions are excluded since they constitute suboptimal options. This task can be visualized as traversing a search tree in which each level corresponds to a switch position of $\boldsymbol{U}$ and with every node having as many siblings as there are output levels for one phase leg, e.g., three siblings for a 3L inverter. As a last step, the algorithm needs to be implemented in a real-time control system. In summary, the sphere decoder can be partitioned into the following steps:

1) reformulation as ILS;
2) calculation of unconstrained solution and initial radius;
3) search for optimal integer solution;
4) real-time implementation.

Several improvements have been proposed to reduce the computational complexity and with that facilitate the real-time implementation of the sphere decoder. In [125], the previously mentioned ILS is restructured by applying a lattice reduction algorithm to achieve a faster convergence of the SDA. The problem of increasing computational burden during transient events is tackled in [126] and [127] by proposing a projection algorithm of the initially calculated radius. Recently, several search strategies have been suggested to speed up the iterative search process: in [128], a segmentation and parallel traversing of the search tree is introduced, while in [129] and [130], a heuristic method called K-best SDA is introduced into the field of power electronics, which searches the K most promising paths instead of traversing the search tree in depth-first manner. Both methods are combined in [131].

One of the major drawbacks of the sphere decoder is that it is only applicable if the prediction model is a linear time-invariant systems. For this reason, the authors in [120] and [132] proposed an algorithm that maps output constraints to input constraints, effectively removing the "violating" candidates from the feasible set, such that the SDA is still applicable. To further expand the applicability to nonlinear systems, linearization approaches have been proposed in [133] and [134] with the goal to predict and control the nonlinear behavior of the NP potential of a 3L-NPC inverter. First investigations on the robustness of the SDA to parameter mismatches were presented in [135] and [136] and followed-up by an online parameter estimation for the SDA in [137].

To the authors' best knowledge, the first implementation of the SDA for MLI was realized on an FPGA in [138] and [139], allowing for a sampling interval of 25 μs for a 3L-NPC inverter with an RL load achieving a horizon length of $N_p = 5$. In contrast to that, in [140], [141], [142], and [143], a high-level synthesis tool is used to generate the VHDL code directly from C++, achieving $N_p = 3$ for a 3L-NPC driving an induction machine at a sampling interval of 25 μs . The implementations presented in [128], [130], and [131] control

TABLE V
STATE-OF-THE-ART IMPLEMENTATIONS OF SDA

Ref.	T_s in µs	max. N_p	Converter—Load	Control-HW
[138]	25	5	3L-NPC—RL	FPGA
[145]	50	3	2L-VSI—PMSM	dSPACE
[127]	125	4	3L-HB—IM	dSPACE
[143]	25	3	3L-NPC—IM	FPGA
[130]	50	5	2L-VSI—UPS	FPGA
[131]	50	7	2L-VSI—UPS	FPGA

a UPS system consisting of a 2L inverter[3] (2L-VSI) with an LC filter connected to an RL load. The SDA was also implemented on dSPACE systems [127], [144], [145], with the limitations that either the sampling interval is long ($>100\,\mu s$) [127], [144], which reduces the switching granularity [59], or a 2L inverter is considered [145], implying that the number of the candidate solutions and, thus, the complexity of the control problem are relatively small. The common implementations of the SDA are summarized in Table V.

b) Other methods: On the other hand, when the optimization problem underlying FCS-MPC is subject to nonlinear constraints, to facilitate its real-time implementation, researchers resort to strategies that simplify the optimization problem at hand by either reformulating the objective function, adopting heuristics or by restricting the feasible set [42], [50], [59], [146], [147], [148]. Nevertheless, differently from the sphere decoder, there are cases where such methods impact the optimality of the calculated solutions, with a negative impact on the system performance. For instance, to avoid the tuning procedure and reduce the computational burden to solve the optimization problem, a simplified FCS-MPC approach is to consider multiple objective functions, each with a single term. The latter are minimized separately one after another, i.e., in a *sequential* manner (see, e.g., [89] and [149]).

Likewise, a straightforward method to keep the computational cost of the optimization process to a minimum is to round (i.e., quantize) the aforementioned *unconstrained* solution $\boldsymbol{U}_{\text{unc}}$ [59]. This means that the entries of the related $\boldsymbol{U}_{\text{unc}}$ are rounded componentwise to the nearest integer of $\boldsymbol{\mathcal{U}}$ (see, e.g., [115] and [150]). Another common approach is to limit the search space, i.e., to reduce the number of candidate solutions to be considered adopting one of the methods denoted in Section III-A.

IV. LYAPUNOV-BASED DIRECT MPC

A. Preliminaries

The Lyapunov direct method has been widely employed in the development of controllers for power electronic applications. In this section, we highlight recent research that integrates the direct Lyapunov method with FCS-MPC. Lyapunov-based MPC is used to improve system stability for bridge converters [151], [152], [153], [154], multilevel converters [87], [155], [156], [157], and drive applications [158], [159], [160], [161], [162].

In [156], a gain-free Lyapunov-based MPC is presented for nested NPC converters. A finite set of control candidates is generated after eliminating the states that make the Lyapunov function nondefinite negative. Since the application of the short-listed control input candidates does not result in an appropriate output state, duty cycle control is also incorporated into the control system. In addition, the cost function of the MPC is designed using fuzzy-logic-based multiobjective optimization. Although the controller achieves satisfactory steady-state error, fast response, and lower average switching frequency compared to classical MPC, its complex design compromises the inherent simplicity, which is a key advantage of MPC.

[3]This concept could be extended to MLIs and is, therefore, listed here.

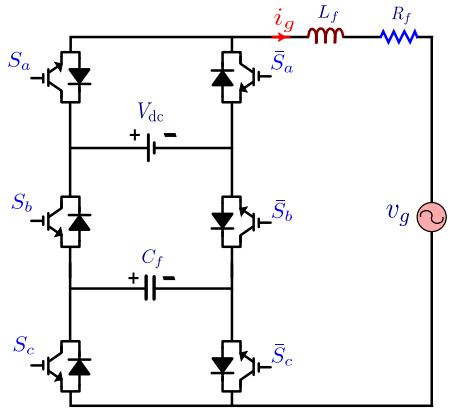

Fig. 16. Grid-connected PUC7 inverter.

For the PUC7 converter [101], [102], the cost function of the classical FCS-MPC is replaced by a Lyapunov-based cost function that eliminates the need for gain tuning and avoids the requirement for additional adjustments and/or controllers. The inhomogeneous terms of the cost function are lumped after eliminating the common term thanks to the direct Lyapunov method. Similar research has used the same design concept for PUC7 rectifiers [102], T-type rectifiers [153], [163], interleaved NPC converters [157], and three-phase four-arm modular multilevel converters [164].

B. Case Study: PUC7 Grid-Connected Inverter

In order to illustrate the design procedure of Lyapunov MPC (LMPC), the PUC7 inverter shown in Fig. 16 is considered as a study example. The cornerstone of the controller design in [101] is to evaluate the performance of the system from a stability perspective, keeping the system stable in the first place. The derivative of the Lyapunov function (i.e., the cost function) should be negative for all time points under different operating conditions. The cost function has no gains, and it is given as

$$\dot{V}(\boldsymbol{x}) = \frac{1}{L_g}\left\{x_1\left(s_1 V_{\text{dc}} + s_2 v_f^* - R_f x_1 - v_i^*\right) - x_2 s_2 i_g^*\right\} \tag{25}$$

where v_f, V_{dc}, and v_g are the capacitor, dc supply, and grid voltages, respectively.

The experimental results during the transient step change of the grid current i_g are shown in Fig. 17, where the controller shows a robust and fast dynamic response during the test and successfully producing seven-level inverter voltage. Compared

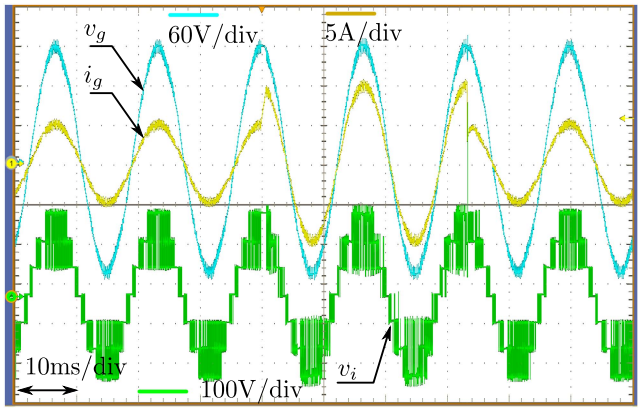

Fig. 17. Experimental results of LMPC for the grid-connected PUC7 inverter.

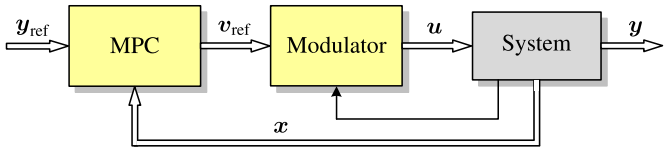

Fig. 18. Block diagram of indirect MPC.

to the classic FCS-MPC, the LMPC demonstrates better robustness against system mismatch and eliminates the need for any gain adjustments.

V. Indirect MPC for MLIs

In contrast to direct MPC methods (such as FCS-MPC), where control and modulation take place in one computational stage, indirect MPC solves these problems in a sequential manner. Hence, indirect MPC computes the control action, e.g., the modulating signal or the duty ratio, which is subsequently fed into a modulator for generation of the switching commands (see Fig. 18). Some indirect MPC methods account for the discrete nature of the switch positions, and hence, the optimization variable is an integer vector. However, most frequently, indirect MPC methods mask the switching nature of the power converter by considering averaged dynamics. In doing so, the optimization variable is a real-valued vector, and the feasible set of the optimization problem underlying indirect MPC is a continuous set. This gives rise to the category of indirect MPC methods that are referred to as CCS-MPC.

A. Continuous-Control-Set MPC

Owing to the real-valued optimization variable and the convexity of the feasible set, the optimization problem underlying CCS-MPC is typically formulated as an unconstrained or constrained QP [165]. Solving the former MPC problem is straightforward as there exists an analytical solution [166]. As a result, the state-feedback control law can be easily computed offline, which greatly simplifies the real-time implementation of such a control strategy.

With regard to CCS-MPC as a constrained QP, even though the complexity of the optimization problem is higher than that

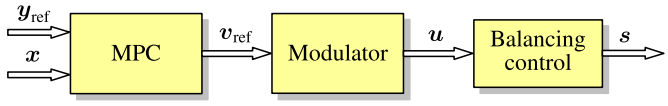

Fig. 19. Block diagram of hierarchical indirect MPC, where s denotes the switching commands sent to the converter.

of the unconstrained QP, its computational complexity is still relatively modest, especially when comparing with FCS-MPC. This is particularly true for multilevel power converters as the computational complexity of CCS-MPC is almost independent of the number of voltage levels, whereas that of FCS-MPC increases exponentially. The above reason, along with the existence of several off-the-self solvers for QPs, facilitates the real-time implementation of CCS-MPC for MLIs [18], [19], [121], [167], [168], [169], [170].

For CCS-MPC to be formulated as a QP, however, the model of the system should be linear, i.e., the discrete-time state-space prediction model should be of the form

$$\boldsymbol{x}(k+1) = \boldsymbol{A}\boldsymbol{x}(k) + \boldsymbol{B}\boldsymbol{u}(k) \tag{26a}$$

$$\boldsymbol{y}(k) = \boldsymbol{C}\boldsymbol{x}(k) \tag{26b}$$

where $\boldsymbol{x} \in \mathbb{R}^{n_x}$ is the state of the system, $\boldsymbol{u} \in \mathbb{R}^{n_u}$ stands for its input, and $\boldsymbol{y} \in \mathbb{R}^{n_y}$ is the system output, with $n_x, n_u, n_y \in \mathbb{N}^+$. This prerequisite introduces a challenge in the controller design as multilevel power converters are typically bilinear systems, i.e., their state-update function is of the form [24]

$$\boldsymbol{f}\left(\boldsymbol{x}(k+1), \boldsymbol{u}(k)\right) = \left(\boldsymbol{A}_1 + \boldsymbol{A}_2\boldsymbol{u}(k)\right)\boldsymbol{x}(k) + \boldsymbol{B}\boldsymbol{u}(k)\,. \tag{27}$$

A way to address this challenge is by locally linearizing the dynamics of the system [18]. This approach, however, introduces a significant computational overhead as it needs the linearization to be performed at every iteration of the controller. An alternative is to introduce reduced-order linear models [171]. In doing so, relatively complicated models can result that do not always fully capture the dynamics of the system. Hence, to meet all the control objectives of interest, a hierarchical control structure is adopted, where the lower layer is typically designed to tackle additional control objectives, such as the voltage balancing of floating capacitors (see Fig. 19). Nevertheless, as this modeling approach requires significantly less computational resources, it is the one usually employed [168], [169].

The aforementioned hierarchical control structure, combined with the existence of a dedicated modulator, introduces an additional disadvantage of indirect MPC. Specifically, the fact that control and modulation are performed in a uncoordinated manner implies that the hardware of the system is not fully utilized as the system may not operate at its physical limits. To overcome this, and ensure the best possible behavior of the system, it is common practice to design explicit constraints in CCS-MPC. To this aim, constraints that relate to actuation limitations (e.g., on the control input) are implemented as *hard* constraints to ensure that the inherent system limitations are fully respected. On the other hand, constraints on the system state/output, which typically relate to physical and/or safety limitations, are usually implemented as *soft* constraints to avoid numerical and/or feasibility issues. In doing so, such constraints

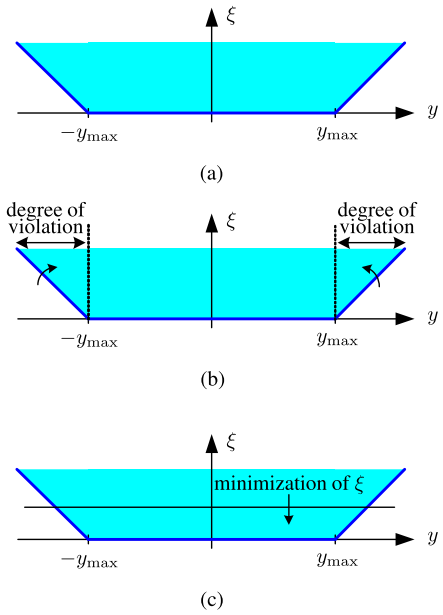

Fig. 20. Example of soft constraints on an output variable y. By minimizing the introduced slack variable ξ, the violation of the constraints is avoided as much as possible. (a) Feasible space of the slack variable ξ. (b) Effect of the degree of constraint violation on the feasible space of ξ. (c) Minimization of the slack variable.

can be violated, but the controller aims to minimize—if not totally eliminate—that violation, as exemplified in Fig. 20. To do so, the degree of their violation, usually modeled by slack variables, is included in the objective function of the CCS-MPC problem [172]. Even though this increases the dimension of the optimization problem, the associated computational cost is relatively small. Hence, the real-time implementation of CCS-MPC with soft constraints is still feasible.

B. Deadbeat MPC

1) Preliminaries: DB-MPC techniques (also called feedback compensation strategies) have been attracting an increased interest in discrete-time dynamic systems' applications. DB-MPC techniques typically use a discretized model of the system to compute the required control actions for a fast transient and zero steady-state error [173], [174], [175]. Therefore, such control techniques have been considered as fast and accurate discrete-time control strategies while characterized by high sensitivity to parameters' variations (changes in the model parameters might lead to oscillatory responses/ringing which is considered as the main drawback of deadbeat control techniques). DB-MPC approaches are commonly used in high dynamics (reference reached within two sampling times). Mostly, these approaches are inspired from the conventional MPC [176] and active filtering techniques [177], [178] to control the output current of the inverter. Moreover, DB-MPC has also been proposed in [174] and [175] to deal with multiple objective control challenges. Kumar and Kim [179] presented a modified deadbeat current controller, based on poles placement, to control the output current and input capacitors' voltage of a hybrid multilevel switching converter. The presented results are very promising

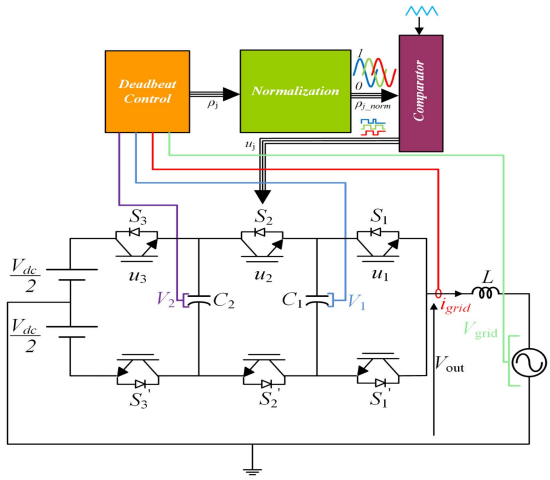

Fig. 21. Normalized DB-MPC technique for a grid-connected 4L-FCI.

for Ring Magnet Power Supply applications as the proposed controller can track random references such as triangular and dc-biased sinusoidal references. An enhanced DB-MPC technique (using the predicted value of the output voltage to substitute the inverter voltage sensor) for the direct power control of a grid-tied switched capacitor MLI was proposed in [180] with including, at each switching cycle, the voltage loss component in the calculated voltage reference. Similarly, a deadbeat predictive controller was proposed in [181] to control an active front-end rectifier based on the 3L-NPC topology. The $\alpha - \beta$ voltage references are computed by the proposed controller to minimize the tracking errors of the active and reactive powers. Then, the transformed abc voltage references are fed to a phase disposition PWM approach for gate pulse generation. A DB-MPC combined with a nearest level modulation approach was proposed in [175], to reduce the circulating current in MMC applications. The suggested control strategy presented a high ability to manage large steady-state circulating current harmonics, superior dynamic performance, while granting the rejection of ac disturbances. Moreover, a dual-objective DB-MPC technique was applied to control a single-phase MMC (minimize the circulating current and track the sinusoidal output current reference) in [182] by governing the upper and lower arm voltages.

2) Case Study: Generally, deadbeat controllers require the minimum steps to reach the desired values. However, depending on the order of the system to be controlled, at least two steps might be required to realize practical and safe operation (typically N samples for an N-order system). Thus, one of the most challenges of deadbeat controllers (based on direct plant inversions) is the fact that the computed actuation signals might go very high and unbounded internal states are introduced (very aggressive and optimistic techniques) when the desired value cannot be reached within the selected sampling time, which leads to saturation in real-time implementation. Thus, Trabelsi et al. [174] proposed a normalized DB-MPC approach. The authors achieved a multiobjective control of a 4L-FC inverter (FCI) (see Fig. 21) by feeding a sinusoidal grid current at unity power factor while regulating the capacitors' voltages around

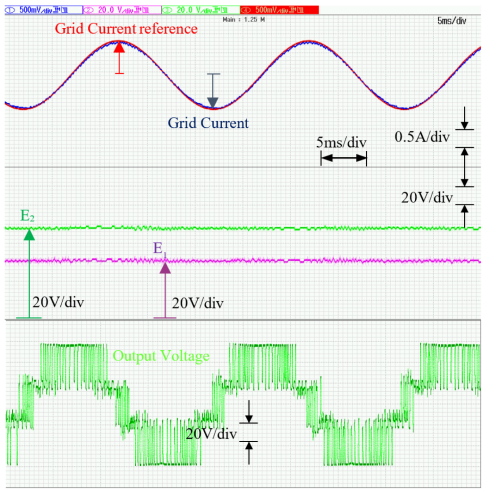

Fig. 22. Normalized DB-MPC technique for a grid-connected 4L-FCI.

their references. The proposed approach allows the normalization of the generated duty cycles to the common base ([0 1]) when the objective is inaccessible during the sampling time

$$d_k = A_{X_k}^{-1}\left(\frac{1}{T_s}(X_k^* - X_k) - B\right) \tag{28}$$

where d_k regroups the computed duty cycles, A_{X_k} is the state matrix (varying according to the variations of the state variables), and B represents the input matrix. The upper part of Fig. 22 shows the experimental grid current against its sinusoidal reference. The middle part shows the high steady-state performance of the capacitors' voltages tracking, while the lower part depicts the 4L output voltage waveform.

VI. Model Uncertainty and Observer Design

A. Preliminaries

Both direct and indirect MPC controllers rely on the MLI models that are used for predictions of system responses to applied actuation in all possible operating conditions. These models serve as a foundation for calculating the optimal actuation. Various types of models can be used to describe the inverter behavior, but the most common ones are based on the discretization of the continuous filter model in accordance with the used sampling time.

B. Model Uncertainty Mitigation Approaches

An ideal scenario would be to have a perfectly accurate model, but this is not possible in practice. For instance, the values of filter parameters change both with the operating conditions and with time; semiconductor switches do not turn ON and OFF instantaneously, while system measurements usually contain a certain amount of noise. For all these reasons, it is important that the MPC algorithms are robust to uncertainties of filter parameters, measurements, and system models. This subsection examines the inherent robustness to uncertainties of prominent MPC methods when applied to MLIs and then reviews several approaches intentionally designed to improve the robustness.

FCS-MPC algorithms are, in general, robust to parameter uncertainty. Earlier studies have shown that acceptable performance is kept under moderate parameter mismatch, while that fundamental operation is not lost even under extreme mismatches [183]. There is also an intuitive explanation for this phenomenon. Namely, since the FCS-MPC algorithm knows the voltage associated with each switch configuration *a priori*, it only evaluates them based on the error of filter variables, which is defined in the cost function. In this context, even if it has wrong values of parameters, it will still be able to choose the actuation that leads to the correct trajectory (albeit it may not be optimal). This is because regardless of the parameter values, the algorithm will always know whether the actuation voltage will lead to rise or fall of the voltages and currents. This explains the fact that as parameter uncertainty increases, the control trajectories will deviate from the optimal ones more and more, but the fundamental operation of the control system is preserved. Similar conclusions concerning robustness can also be derived for machine-learning-based surrogates of FCS-MPC controllers [184].

As for the CCS-MPC, it is well known that these approaches are conceptually equivalent to the state-feedback controllers [185], [186]. In this context, the robustness properties are similar to the state feedback controllers and can be formally studied using classical control theory. Nonetheless, Majmunovic et al. [187] have also made an experimental investigation, about the influence of the filter parameter uncertainty on the performance of a voltage source converter in the UPS mode of operation. The tests have been conducted for $\pm 40\%$ parameter variation from the nominal value. From the presented results, it could have been noted that the controller is robust to parameter uncertainties, albeit somewhat less robust compared to FCS-MPC. This in accordance to intuition as well since CCS-MPC for a comparable systems usually operates at several times lower sampling frequency.

C. Observer Design Approaches

Another important issue to consider is the cost of implementing the MPC controllers. Namely, although MPC can, in general, achieve superior performance compared to conventional linear cascaded control systems, this benefit often comes at a higher implementation cost [188]. In particular, MPC strategies in their basic implementation formats usually require a high number of voltage and current sensors, as well as high computing power. In this context, observers can help mitigate some of the sensor cost [189].

Another important application of observers is to estimate the prediction model. Various types of methods have been used for this purpose, from classical observation theory to machine learning. Each of them has its own advantages and disadvantages. For instance, classical linear models are well understood, and each parameter in them corresponds to interpretable quantity [190]. However, such models also have limited ability to learn potentially nonlinear parameter drifts and other imperfections in the system. Therefore, it can be concluded that for systems with many parameters such as the ones often found in MLIs,

TABLE VI
ASSESSMENT OF MOST COMMON MPC METHODS FOR MLIS

Method	Computational Burden	Design Complexity	Multiobjective Handling	Gains/Weighting Factors	Explicit Modulator	Switching Frequency	Parameter Robustness	Steady-state Performance	Dynamic Performance
Conventional FCS-MPC	✓	✓✓	✓✓	✗✗	Not required	Variable	✗	✗	✓
Long-Horizon FCS-MPC	✗	✓	✓✓	✗	Not required	Variable	✗✗	✓	✓
Lyapunov MPC	✓	✓✓	✗✗	✓✓	Not required	Variable	✓	✗	✓
MP2C	✗	✓	✓✓	✗✗	Not required	Fixed	✗	✓	✓
OSS-MPC	✗✗	✗✗	✓✓	✗✗	Not required	Fixed	✗	✓✓	✓✓
CCS-MPC	✓	✓	✓✓	✗	required	Fixed	✗	✓✓	✓
Deadbeat MPC	✓✓	✓✓	✗✗	N/A	required	Fixed	✗✗	✓✓	✓
Classic PI-PWM	✓✓	✓	✗✗	✗✗	required	Fixed	✓✓	✓✓	✗✗

* Scaled from best (✓✓) to worst (✗✗).

machine learning models are often more suitable [191], [192]. Nonetheless, it should be noted that machine learning models are essentially black box, so one needs to pay special attention to make sure that the model provides expected behavior when exposed to all possible operating conditions. Statistical model checking is a good methodology for this purpose [193].

On the other hand, computing power needs can be reduced by smart implementations of MPC strategies. The most notable ones in the context of MLIs are long-horizon MPC, sequential MPC, and machine learning MPC surrogates, all of which have been investigated in detail in previous sections in this article.

VII. COMPARISON OF MPC METHODS

In this section, a brief qualitative comparison between the common MPC methods for MLIs is presented and summarized in Table VI. The classic PI controller in conjunction with a PWM stage is also included in the comparison [13], [194]. The evaluation encompasses various metrics, including computational burden, design complexity, capability to accommodate multiple control objectives, efforts required for tuning WFs and controller gains, switching frequency, sensitivity to parameter mismatches, steady-state performance, and dynamic performance.

Simplicity of design and ability to easily include multiple objectives are obvious advantages of conventional FCS-MPC; however, the need for a WF for each objective with the accompanying tuning efforts is a challenge in this scheme. Also, the variable switching frequency makes this method not recommended for grid-connected applications due to the difficulty of the filter design. Long-horizon MPC can achieve better steady-state performance; however, the computational burden increases exponentially as the number of prediction steps N_p increases.

Lyapunov-based MPC is a type of controller that uses a discrete form of the derivative of the positive Lyapunov cost function to ensure system stability and robustness. It is similar to conventional FCS-MPC with optimized weights, achieved by canceling the common term of the errors. However, this method is not suitable for systems with multiple constraints, and there is no detailed stability analysis available for this type of controller.

M2PC and OSS-MPC are two approaches aimed at enhancing the steady-state performance of the conventional FCS-MPC and operating at a fixed switching frequency. However, while offering these advantages, these approaches introduce additional calculation loads and deviate from the design simplicity inherent in the traditional method.

Indirect MPC, in its version of CCS-MPC, exhibits the characteristic advantages of MPC, such as the ability to handle multiple objectives and explicit system constraints in a straightforward manner. At the same time, the inherent disadvantages of MPC appear in this derivative as well. Hence, the existence of multiple WFs—which can be more than in FCS-MPC due to the presence of slack variables—can complicate the controller tuning, while the lack of an integrating element can make the controller susceptible to model deviations, parameter uncertainties, etc. Nevertheless, since CCS-MPC is formulated as a QP, its computational complexity can be relatively modest, even when a long horizon is employed, while the presence of a dedicated modulator results in a fixed switching frequency. These advantages make CCS-MPC particularly attractive for a wide range of applications, such as grid-connected converters or applications where higher switching frequencies are required.

DB-MPC exhibits excellent steady-state performance and constant switching frequency, similar to that of a linear PI controller, as both the methods employ a modulation stage. However, effectively addressing multiple objectives can be challenging, although it can be achieved to some extent by leveraging the available redundant states of the MLI topology within the modulation stage. While the DB-MPC has high dynamic performance and avoids the problematic tuning associated with the classical PI controller, one drawback is its high sensitivity to model parameter mismatch.

VIII. FUTURE TRENDS

MPC has demonstrated a high capability to handle the challenging multiobjective control problems of MLI applications with easy implementation, simplicity, and high dynamic performance. Although tremendous progress has been achieved over the last decade, MPC still has some challenges that represent open research topics.

Several works have been reported to reduce the computational efforts of direct MPC for MLI applications. However, most of them rely on offline calculations and stored LUTs, which require high storage space. In addition, some computationally efficient schemes suffer from a significant deterioration in the performance and/or increased complexity compared to the conventional method. Therefore, reducing calculations without

degrading control performance or without storing numerous LUTs is still an open research point, especially for high-level MLIs ($N_{\text{level}} \geq 5$). Solving this research question will bring tangible benefits from the industry perspective because this will allow the practical implementation at high sampling frequencies with inexpensive commercial microprocessors.

With OSS-MPC, the heavy computational problem becomes more severe since it is the most computationally demanding subset of direct MPC [195]. During the optimization process of OSS-MPC, not only the voltage vectors of all the switching sequences are evaluated, but also the dwell time of vectors in the optimal sequence is determined. There is some incipient work to mitigate the acute computational complexity of OSS-MPC with MLIs [196]. In addition, most of the existing research on OSS-MPC with MLIs is limited to single-phase operation or three-phase 3L topologies. Therefore, the extension of OSS-MPC to higher level three-phase topologies requires further investigation with addressing the related issues.

The computational burden remains a challenge for many control algorithms, since the control has to be calculated in real time. This may limit the performance of FCS-MPC, since the sampling time indirectly defines the switching granularity. Another emerging research direction relates to the formulation of the MPC problem. Many of the derived MPC formulations assume linear systems of the form with integer or real-valued inputs. Given that many applications do not meet such a prerequisite, this means that they either have to be linearized or other methods need to be developed and/or solvers employed. To tackle these issues, MPC needs to be addressed as a nonlinear problem.

Moreover, being a multiobjective control technique, the performance of the MPC approach depends mainly on the tedious and time-consuming task of tuning the objectives' WFs to determine their priorities in the control decision. The ANN-based WF optimization can effectively select the optimal values through offline prediction and real-time adjustment. With the help of dynamic adjustment of WFs, FCS-MPC can realize the desirable performance. Future research may concentrate on the ANN optimization using the FPGA/ARM, in order to realize the autotuning of WFs without increasing the computational burden of FCS-MPC. In addition, the cost and logic resources of the microcontrollers (online autotuning computation requirements) should be taken into consideration in the industrial applications. In the same regard, MPC without WFs for MLIs can eliminate the complex tuning process, but more research should be devoted to how to avoid the suboptimal problems. Compared with the MPC with a regular cost function, it should be proved that weighting factorless MPC is able to provide the same or even better control performance.

Due to a larger number of components, the control algorithms for MLIs have to also focus on the reliability of the components. Especially, the FCS-MPC has a lot of freedom in the cost function design to include objectives that can improve the reliability of the MLIs, something that is not very straightforward for conventional linear control algorithms. The challenge here lies in finding the optimum stress distribution of the components (both the semiconductor devices and capacitors) that will ensure the longest lifetime of the converter.

Though Lyapunov-based MPC features simplicity and does not require gain tuning, relation between passive components used in the controlled model and the controller performance is still to be investigated. Moreover, stability analysis and using a discrete Lyapunov cost function instead of discretizing the continuous form are still not studied in the literature.

IX. Conclusion

MPC has proven itself as a promising control method to handle the challenging multiple-objective control problem of MLIs. Over the last decade, substantial improvements have been introduced to MPC for MLI applications including computational burden reduction, cost function design, WF selection, operation at fixed switching frequency, modeling accuracy, and long-horizon implementation. This article presented the fundamentals, operating principles, and technical challenges of the MPC for MLIs, focusing on FCS-MPC as the most popular approach for MLIs. The advances and effective solutions to each challenge were discussed. Some prominent concepts were validated and compared to evaluate their performance. Finally, the ongoing research points and future trends were presented.

References

[1] J. Rodriguez, J.-S. Lai, and F. Z. Peng, "Multilevel inverters: A survey of topologies, controls, and applications," *IEEE Trans. Ind. Electron.*, vol. 49, no. 4, pp. 724–738, Aug. 2002.

[2] K. K. Gupta, A. Ranjan, P. Bhatnagar, L. K. Sahu, and S. Jain, "Multilevel inverter topologies with reduced device count: A review," *IEEE Trans. Power Electron.*, vol. 31, no. 1, pp. 135–151, Jan. 2016.

[3] A. M. S. Ali, H. Van Khang, K. G. Robbersmyr, M. Norambuena, and J. Rodriguez, "Novel three-phase multilevel inverter with reduced components for low-and high-voltage applications," *IEEE Trans. Ind. Electron.*, vol. 68, no. 7, pp. 5978–5989, Jul. 2021.

[4] J. Richalet, A. Rault, J. Testud, and J. Papon, "Model predictive heuristic control: Applications to industrial processes," *Automatica*, vol. 14, no. 5, pp. 413–428, 1978.

[5] J. Holtz, "A predictive controller for the stator current vector of ac machines fed from a switched voltage source," in *Proc. IEE Jpn. Int. Power Electron. Conf.*, 1983, pp. 1665–1675.

[6] D. F. Schroder and R. Kennel, "Model-control PROMC—A new control strategy with microcomputer for drive applications," *IEEE Trans. Ind. Appl.*, vol. IA-21, no. 5, pp. 1162–1167, Sep. 1985.

[7] S. Kouro, P. Cortés, R. Vargas, U. Ammann, and J. Rodríguez, "Model predictive control—A simple and powerful method to control power converters," *IEEE Trans. Ind. Electron.*, vol. 56, no. 6, pp. 1826–1838, Jun. 2009.

[8] N. Oikonomou, C. Gutscher, P. Karamanakos, F. D. Kieferndorf, and T. Geyer, "Model predictive pulse pattern control for the five-level active neutral-point-clamped inverter," *IEEE Trans. Ind. Appl.*, vol. 49, no. 6, pp. 2583–2592, Nov./Dec. 2013.

[9] J. Scoltock, T. Geyer, and U. K. Madawala, "A model predictive direct current control strategy with predictive references for MV grid-connected converters with LCL-filters," *IEEE Trans. Power Electron.*, vol. 30, no. 10, pp. 5926–5937, Oct. 2014.

[10] K. Antoniewicz, M. Jasinski, M. P. Kazmierkowski, and M. Malinowski, "Model predictive control for three-level four-leg flying capacitor converter operating as shunt active power filter," *IEEE Trans. Ind. Electron.*, vol. 63, no. 8, pp. 5255–5262, Aug. 2016.

[11] C. R. Baier, R. O. Ramirez, E. I. Marciel, J. C. Hernández, P. E. Melín, and E. E. Espinosa, "FCS-MPC without steady-state error applied to a grid-connected cascaded H-bridge multilevel inverter," *IEEE Trans. Power Electron.*, vol. 36, no. 10, pp. 11785–11799, Oct. 2021.

[12] T. Geyer and S. Mastellone, "Model predictive direct torque control of a five-level ANPC converter drive system," *IEEE Trans. Ind. Appl.*, vol. 48, no. 5, pp. 1565–1575, Sep./Oct. 2012.

[13] R. Vargas, P. Cortés, U. Ammann, J. Rodríguez, and J. Pontt, "Predictive control of a three-phase neutral-point-clamped inverter," *IEEE Trans. Ind. Electron.*, vol. 54, no. 5, pp. 2697–2705, Oct. 2007.

[14] Y. Yang et al., "Model predictive current control with low complexity for single-phase four-level hybrid-clamped converters," *IEEE Trans. Transp. Electrific.*, vol. 7, no. 3, pp. 983–999, Sep. 2021.

[15] I. Harbi, M. Abdelrahem, M. Ahmed, and R. Kennel, "Reduced-complexity model predictive control with online parameter assessment for a grid-connected single-phase multilevel inverter," *Sustainability*, vol. 12, no. 19, 2020, Art. no. 7997.

[16] Y. Yang, J. Pan, H. Wen, Z. Zhang, Z. Ke, and L. Xu, "Double-vector model predictive control for single-phase five-level actively clamped converters," *IEEE Trans. Transp. Electrific.*, vol. 5, no. 4, pp. 1202–1213, Dec. 2019.

[17] L. Tarisciotti, P. Zanchetta, A. Watson, S. Bifaretti, and J. C. Clare, "Modulated model predictive control for a seven-level cascaded H-bridge back-to-back converter," *IEEE Trans. Ind. Electron.*, vol. 61, no. 10, pp. 5375–5383, Oct. 2014.

[18] G. Darivianakis, T. Geyer, and W. van der Merwe, "Model predictive current control of modular multilevel converters," in *Proc. IEEE Energy Convers. Congr. Expo.*, 2014, pp. 5016–5023.

[19] D. Zhou, S. Yang, and Y. Tang, "Model-predictive current control of modular multilevel converters with phase-shifted pulsewidth modulation," *IEEE Trans. Ind. Electron.*, vol. 66, no. 6, pp. 4368–4378, Jun. 2019.

[20] D. Zhou, Z. Quan, and Y. Li, "Hybrid model predictive control of ANPC converters with decoupled low-frequency and high-frequency cells," *IEEE Trans. Power Electron.*, vol. 35, no. 8, pp. 8569–8580, Aug. 2020.

[21] F. Kieferndorf, M. Basler, L. Serpa, J.-H. Fabian, A. Coccia, and G. Scheuer, "ANPC-5L technology applied to medium voltage variable speed drives applications," in *Proc. IEEE Int. Symp. Power Electron., Elect. Drives, Autom. Motion*, 2010, pp. 1718–1725.

[22] V. Yaramasu and B. Wu, *Model Predictive Control of Wind Energy Conversion Systems*. Hoboken, NJ, USA: Wiley, 2016.

[23] S. Vazquez, J. Rodriguez, M. Rivera, L. G. Franquelo, and M. Norambuena, "Model predictive control for power converters and drives: Advances and trends," *IEEE Trans. Ind. Electron.*, vol. 64, no. 2, pp. 935–947, Feb. 2016.

[24] P. Karamanakos, E. Liegmann, T. Geyer, and R. Kennel, "Model predictive control of power electronic systems: Methods, results, and challenges," *IEEE Open J. Ind. Appl.*, vol. 1, pp. 95–114, 2020.

[25] J. Rodriguez and P. Cortes, *Predictive Control of Power Converters and Electrical Drives*. Hoboken, NJ, USA: Wiley, 2012.

[26] Y. Yang et al., "Low complexity finite-control-set MPC based on discrete space vector modulation for T-type three-phase three-level converters," *IEEE Trans. Power Electron.*, vol. 37, no. 1, pp. 392–403, Jan. 2022.

[27] Y. Yang et al., "Multiple-voltage-vector model predictive control with reduced complexity for multilevel inverters," *IEEE Trans. Transp. Electrific.*, vol. 6, no. 1, pp. 105–117, Mar. 2020.

[28] A. G. Yepes, F. D. Freijedo, J. Doval-Gandoy, Ó. López, J. Malvar, and P. Fernandez-Comesana, "Effects of discretization methods on the performance of resonant controllers," *IEEE Trans. Power Electron.*, vol. 25, no. 7, pp. 1692–1712, Jul. 2010.

[29] D. Zhou, Z. Quan, Y. Li, and J. Zou, "A general constant-switching-frequency model-predictive control of multilevel converters with quasi-PS-PWM/LS-PWM output," *IEEE Trans. Power Electron.*, vol. 35, no. 11, pp. 12429–12441, Nov. 2020.

[30] T. J. Vyncke, S. Thielemans, and J. A. Melkebeek, "Finite-set model-based predictive control for flying-capacitor converters: Cost function design and efficient FPGA implementation," *IEEE Trans. Ind. Inform.*, vol. 9, no. 2, pp. 1113–1121, May 2013.

[31] M. Novak, V. Ferreira, M. Andresen, T. Dragicevic, F. Blaabjerg, and M. Liserre, "FS-MPC based thermal stress balancing and reliability analysis for NPC converters," *IEEE Open J. Power Electron.*, vol. 2, pp. 124–137, 2021.

[32] J. Kolb, F. Kammerer, M. Gommeringer, and M. Braun, "Cascaded control system of the modular multilevel converter for feeding variable-speed drives," *IEEE Trans. Power Electron.*, vol. 30, no. 1, pp. 349–357, Jan. 2015.

[33] P. Karamanakos and T. Geyer, "Model predictive torque and flux control minimizing current distortions," *IEEE Trans. Power Electron.*, vol. 34, no. 3, pp. 2007–2012, Mar. 2019.

[34] V. Yaramasu and B. Wu, "Model predictive decoupled active and reactive power control for high-power grid-connected four-level diode-clamped inverters," *IEEE Trans. Ind. Electron.*, vol. 61, no. 7, pp. 3407–3416, Jul. 2014.

[35] J. Scoltock, T. Geyer, and U. K. Madawala, "Model predictive direct power control for grid-connected NPC converters," *IEEE Trans. Ind. Electron.*, vol. 62, no. 9, pp. 5319–5328, Sep. 2015.

[36] J. Jongudomkarn, J. Liu, and T. Ise, "Virtual synchronous generator control with reliable fault ride-through ability: A solution based on finite-set model predictive control," *IEEE Trans. Emerg. Sel. Topics Power Electron.*, vol. 8, no. 4, pp. 3811–3824, Dec. 2020.

[37] M. R. Nasiri, S. Farhangi, and J. Rodríguez, "Model predictive control of a multilevel CHB STATCOM in wind farm application using Diophantine equations," *IEEE Trans. Ind. Electron.*, vol. 66, no. 2, pp. 1213–1223, Feb. 2019.

[38] P. Cortés, G. Ortiz, J. I. Yuz, J. Rodríguez, S. Vazquez, and L. G. Franquelo, "Model predictive control of an inverter with output LC filter for UPS applications," *IEEE Trans. Ind. Electron.*, vol. 56, no. 6, pp. 1875–1883, Jun. 2009.

[39] P. Karamanakos, T. Geyer, and R. Kennel, "On the choice of norm in finite control set model predictive control," *IEEE Trans. Power Electron.*, vol. 33, no. 8, pp. 7105–7117, Aug. 2018.

[40] V. Yaramasu and B. Wu, "Predictive control of a three-level boost converter and an NPC inverter for high-power PMSG-based medium voltage wind energy conversion systems," *IEEE Trans. Power Electron.*, vol. 29, no. 10, pp. 5308–5322, Oct. 2014.

[41] O. Kukrer, "Discrete-time current control of voltage-fed three-phase PWM inverters," *IEEE Trans. Power Electron.*, vol. 11, no. 2, pp. 260–269, Mar. 1996.

[42] T. Geyer and D. E. Quevedo, "Multistep finite control set model predictive control for power electronics," *IEEE Trans. Power Electron.*, vol. 29, no. 12, pp. 6836–6846, Dec. 2014.

[43] P. Cortes, A. Wilson, S. Kouro, J. Rodriguez, and H. Abu-Rub, "Model predictive control of multilevel cascaded H-bridge inverters," *IEEE Trans. Ind. Electron.*, vol. 57, no. 8, pp. 2691–2699, Aug. 2010.

[44] C. Xia, T. Liu, T. Shi, and Z. Song, "A simplified finite-control-set model-predictive control for power converters," *IEEE Trans. Ind. Inform.*, vol. 10, no. 2, pp. 991–1002, May 2014.

[45] I. Kim, R. Chan, and S. Kwak, "Model predictive control method for CHB multi-level inverter with reduced calculation complexity and fast dynamics," *IET Electr. Power Appl.*, vol. 11, no. 5, pp. 784–792, 2017.

[46] Y. Yang, H. Wen, M. Fan, M. Xie, and R. Chen, "Fast finite-switching-state model predictive control method without weighting factors for T-type three-level three-phase inverters," *IEEE Trans. Ind. Inform.*, vol. 15, no. 3, pp. 1298–1310, Mar. 2019.

[47] S. R. Mohapatra and V. Agarwal, "Model predictive controller with reduced complexity for grid-tied multilevel inverters," *IEEE Trans. Ind. Electron.*, vol. 66, no. 11, pp. 8851–8855, Nov. 2019.

[48] A. Mora, R. Cárdenas-Dobson, R. P. Aguilera, A. Angulo, F. Donoso, and J. Rodriguez, "Computationally efficient cascaded optimal switching sequence MPC for grid-connected three-level NPC converters," *IEEE Trans. Power Electron.*, vol. 34, no. 12, pp. 12464–12475, Dec. 2019.

[49] Y. Yang et al., "Computationally efficient model predictive control with fixed switching frequency of five-level ANPC converters," *IEEE Trans. Ind. Electron.*, vol. 69, no. 12, pp. 11903–11914, Dec. 2022.

[50] Z. Zhang, C. M. Hackl, and R. Kennel, "Computationally efficient DMPC for three-level NPC back-to-back converters in wind turbine systems with PMSG," *IEEE Trans. Power Electron.*, vol. 32, no. 10, pp. 8018–8034, Oct. 2017.

[51] C. Garcia et al., "FCS-MPC based pre-filtering stage for computational efficiency in a flying capacitor converter," *IEEE Access*, vol. 9, pp. 111039–111049, 2021.

[52] Y. Li, F. Diao, and Y. Zhao, "Simplified two-stage model predictive control for a hybrid multilevel converter with floating H-bridge," *IEEE Trans. Power Electron.*, vol. 36, no. 4, pp. 4839–4850, Apr. 2021.

[53] A. Bahrami, M. Norambuena, M. Narimani, and J. Rodriguez, "Model predictive current control of a seven-level inverter with reduced computational burden," *IEEE Trans. Power Electron.*, vol. 35, no. 6, pp. 5729–5740, Jun. 2020.

[54] J. Ma, W. Song, X. Wang, F. Blaabjerg, and X. Feng, "Low-complexity model predictive control of single-phase three-level rectifiers with unbalanced load," *IEEE Trans. Power Electron.*, vol. 33, no. 10, pp. 8936–8947, Oct. 2018.

[55] I. Harbi, M. Ahmed, J. Rodriguez, R. Kennel, and M. Abdelrahem, "Low-complexity finite set model predictive control for split-capacitor ANPC inverter with different levels modes and online model update," *IEEE Trans. Emerg. Sel. Topics Power Electron.*, vol. 11, no. 1, pp. 506–522, Feb. 2023.

[56] I. Harbi, M. Abdelrahem, M. Ahmed, and R. Kennel, "Weighting factorless reduced-complexity FS-MPC for modified packed U-cell inverter topology," in *Proc. IEEE Int. Exhib. Conf. Power Electron., Intell. Motion, Renewable Energy Energy Manage.*, 2021, pp. 1–8.

[57] J. Liu, S. Cheng, Y. Liu, and A. Shen, "FCS-MPC for a single-phase two-stage grid-connected PV inverter," *IET Power Electron.*, vol. 12, no. 4, pp. 915–922, 2019.

[58] K. K. Monfared, A. Miremad, H. Iman-Eini, and Y. Neyshabouri, "Finite control set model predictive control for static synchronous compensator based on hybrid cascaded H-bridge and neutral point clamped multilevel inverter," *Int. Trans. Elect. Energy Syst.*, vol. 31, no. 2, 2021, Art. no. e12745.

[59] P. Karamanakos and T. Geyer, "Guidelines for the design of finite control set model predictive controllers," *IEEE Trans. Power Electron.*, vol. 35, no. 7, pp. 7434–7450, Jul. 2020.

[60] H. Zhang, Z. Ma, Z. Li, X. Zhang, Z. Liao, and G. Lin, "Multivariable sequential model predictive control of LCL-type grid connected inverter," in *Proc. IEEE Int. Conf. Predictive Control Elect. Drives Power Electron.*, 2021, pp. 777–781.

[61] J. Li et al., "Sequential predictive control with dynamic priority of three-level NPC back-to-back power converters in PMSG wind turbine systems," in *Proc. IEEE Int. Conf. Predictive Control Elect. Drives Power Electron.*, 2021, pp. 462–467.

[62] T. Liu, A. Chen, C. Qin, J. Chen, and X. Li, "Double vector model predictive control to reduce common-mode voltage without weighting factors for three-level inverters," *IEEE Trans. Ind. Electron.*, vol. 67, no. 10, pp. 8980–8990, Oct. 2020.

[63] T. Barth, F. Filsecker, and S. Bernet, "Model predictive control of a hybrid Si/SiC 3L-NPC converter," in *Proc. IEEE 15th Workshop Control Model. Power Electron.*, 2014, pp. 1–6.

[64] M. Novak and F. Blaabjerg, "Model predictive active thermal control strategy for lifetime extension of a 3L-NPC converter for ups applications," in *Proc. IEEE 21st Workshop Control Model. Power Electron.*, 2020, pp. 1–7.

[65] P. Zanchetta, "Heuristic multi-objective optimization for cost function weights selection in finite states model predictive control," in *Proc. IEEE Workshop Predictive Control Elect. Drives Power Electron.*, 2011, pp. 70–75.

[66] P. R. U. Guazzelli, W. C. de A. Pereira, C. M. R. de Oliveira, A. G. de Castro, and M. L. de Aguiar, "Weighting factors optimization of predictive torque control of induction motor by multiobjective genetic algorithm," *IEEE Trans. Power Electron.*, vol. 34, no. 7, pp. 6628–6638, Jul. 2019.

[67] H. Fretes et al., "Pareto optimal weighting factor design of predictive current controller of a six-phase induction machine based on particle swarm optimization algorithm," *IEEE Trans. Emerg. Sel. Topics Power Electron.*, vol. 10, no. 1, pp. 207–219, Feb. 2022.

[68] T. Dragičević and M. Novak, "Weighting factor design in model predictive control of power electronic converters: An artificial neural network approach," *IEEE Trans. Ind. Electron.*, vol. 66, no. 11, pp. 8870–8880, Nov. 2018.

[69] M. Novak, H. Xie, T. Dragicevic, F. Wang, J. Rodriguez, and F. Blaabjerg, "Optimal cost function parameter design in predictive torque control (PTC) using artificial neural networks (ANN)," *IEEE Trans. Ind. Electron.*, vol. 68, no. 8, pp. 7309–7319, Aug. 2021.

[70] C. Yao, Z. Sun, S. Xu, H. Zhang, G. Ren, and G. Ma, "Optimal parameters design for model predictive control using an artificial neural network optimized by genetic algorithm," in *Proc. IEEE 13th Int. Symp. Linear Drives Ind. Appl.*, 2021, pp. 1–6.

[71] F. Donoso, A. Mora, R. Cardenas, A. Angulo, D. Saez, and M. Rivera, "Finite-set model-predictive control strategies for a 3L-NPC inverter operating with fixed switching frequency," *IEEE Trans. Ind. Electron.*, vol. 65, no. 5, pp. 3954–3965, May 2018.

[72] L. M. Caseiro, A. M. Mendes, and S. M. Cruz, "Dynamically weighted optimal switching vector model predictive control of power converters," *IEEE Trans. Ind. Electron.*, vol. 66, no. 2, pp. 1235–1245, Feb. 2019.

[73] S. A. Davari, D. A. Khaburi, and R. Kennel, "An improved FCS–MPC algorithm for an induction motor with an imposed optimized weighting factor," *IEEE Trans. Power Electron.*, vol. 27, no. 3, pp. 1540–1551, Mar. 2012.

[74] X. Li, H. Zhang, M. B. Shadmand, and R. S. Balog, "Model predictive control of a voltage-source inverter with seamless transition between islanded and grid-connected operations," *IEEE Trans. Ind. Electron.*, vol. 64, no. 10, pp. 7906–7918, Oct. 2017.

[75] M. B. Shadmand, S. Jain, and R. S. Balog, "Autotuning technique for the cost function weight factors in model predictive control for power electronic interfaces," *IEEE Trans. Emerg. Sel. Topics Power Electron.*, vol. 7, no. 2, pp. 1408–1420, Jun. 2019.

[76] A. Bhowate, M. Aware, and S. Sharma, "Predictive torque control with online weighting factor computation technique to improve performance of induction motor drive in low speed region," *IEEE Access*, vol. 7, pp. 42309–42321, 2019.

[77] C. A. Rojas, J. R. Rodriguez, S. Kouro, and F. Villarroel, "Multiobjective fuzzy-decision-making predictive torque control for an induction motor drive," *IEEE Trans. Power Electron.*, vol. 32, no. 8, pp. 6245–6260, Aug. 2017.

[78] F. Villarroel, J. R. Espinoza, C. A. Rojas, J. Rodriguez, M. Rivera, and D. Sbarbaro, "Multiobjective switching state selector for finite-states model predictive control based on fuzzy decision making in a matrix converter," *IEEE Trans. Ind. Electron.*, vol. 60, no. 2, pp. 589–599, Feb. 2013.

[79] Z. Zhang, W. Tian, W. Xiong, and R. Kennel, "Predictive torque control of induction machines fed by 3L-NPC converters with online weighting factor adjustment using fuzzy logic," in *Proc. IEEE Transp. Electrific. Conf. Expo.*, 2017, pp. 84–89.

[80] V. P. Muddineni, A. K. Bonala, and S. R. Sandepudi, "Enhanced weighting factor selection for predictive torque control of induction motor drive based on Vikor method," *IET Electr. Power Appl.*, vol. 10, no. 9, pp. 877–888, 2016.

[81] V. P. Muddineni, S. R. Sandepudi, and A. K. Bonala, "Finite control set predictive torque control for induction motor drive with simplified weighting factor selection using Topsis method," *IET Electr. Power Appl.*, vol. 11, no. 5, pp. 749–760, 2017.

[82] S. A. Davari, V. Nekoukar, C. Garcia, and J. Rodriguez, "Online weighting factor optimization by simplified simulated annealing for finite set predictive control," *IEEE Trans. Ind. Inform.*, vol. 17, no. 1, pp. 31–40, Jan. 2021.

[83] R.-J. Wai and L.-C. Shih, "Adaptive fuzzy-neural-network design for voltage tracking control of a dc–dc boost converter," *IEEE Trans. Power Electron.*, vol. 27, no. 4, pp. 2104–2115, Apr. 2012.

[84] X. Liu et al., "Neural predictor-based low switching frequency FCS-MPC for MMC with online weighting factors tuning," *IEEE Trans. Power Electron.*, vol. 37, no. 4, pp. 4065–4079, Apr. 2022.

[85] S. Vazquez et al., "An artificial intelligence approach for real-time tuning of weighting factors in FCS-MPC for power converters," *IEEE Trans. Ind. Electron.*, vol. 69, no. 12, pp. 11987–11998, Dec. 2022.

[86] O. Machado, P. Martín, F. J. Rodríguez, and E. J. Bueno, "A neural network-based dynamic cost function for the implementation of a predictive current controller," *IEEE Trans. Ind. Inform.*, vol. 13, no. 6, pp. 2946–2955, Dec. 2017.

[87] M. Babaie, M. Mehrasa, M. Sharifzadeh, and K. Al-Haddad, "Floating weighting factors ANN-MPC based on Lyapunov stability for seven-level modified PUC active rectifier," *IEEE Trans. Ind. Electron.*, vol. 69, no. 1, pp. 387–398, Jan. 2022.

[88] C. A. Rojas, J. Rodriguez, F. Villarroel, J. R. Espinoza, C. A. Silva, and M. Trincado, "Predictive torque and flux control without weighting factors," *IEEE Trans. Ind. Electron.*, vol. 60, no. 2, pp. 681–690, Feb. 2013.

[89] M. Norambuena, J. Rodriguez, Z. Zhang, F. Wang, C. Garcia, and R. Kennel, "A very simple strategy for high-quality performance of AC machines using model predictive control," *IEEE Trans. Power Electron.*, vol. 34, no. 1, pp. 794–800, Jan. 2019.

[90] E. Kusuma, K. M. R. Eswar, and T. V. Kumar, "An effective predictive torque control scheme for PMSM drive without involvement of weighting factors," *IEEE Trans. Emerg. Sel. Topics Power Electron.*, vol. 9, no. 3, pp. 2685–2697, Jun. 2021.

[91] F. Wang, H. Xie, Q. Chen, S. A. Davari, J. Rodriguez, and R. Kennel, "Parallel predictive torque control for induction machines without weighting factors," *IEEE Trans. Power Electron.*, vol. 35, no. 2, pp. 1779–1788, Feb. 2020.

[92] D. Xiao, M. P. Akter, K. Alam, R. Dutta, S. Mekhilef, and M. F. Rahman, "Cascaded predictive flux control for a 3-L active NPC fed IM drives without weighting factor," *IEEE Trans. Energy Convers.*, vol. 36, no. 3, pp. 1797–1807, Sep. 2021.

[93] H. Makhamreh, M. Trabelsi, O. Kükrer, and H. Abu-Rub, "An effective sliding mode control design for a grid-connected PUC7 multilevel inverter," *IEEE Trans. Ind. Electron.*, vol. 67, no. 5, pp. 3717–3725, May 2020.

[94] M. Xiao, T. Shi, Y. Yan, W. Xu, and C. Xia, "Predictive torque control of permanent magnet synchronous motors using flux vector," *IEEE Trans. Ind. Appl.*, vol. 54, no. 5, pp. 4437–4446, Sep./Oct. 2018.

[95] Z. Song, X. Ma, and R. Zhang, "Enhanced finite-control-set model predictive flux control of permanent magnet synchronous machines with minimum torque ripples," *IEEE Trans. Ind. Electron.*, vol. 68, no. 9, pp. 7804–7813, Sep. 2020.

[96] C. Ma et al., "A novel torque boundary-based model predictive torque control for PMSM without weighting factor," *IEEE Trans. Emerg. Sel. Topics Power Electron.*, vol. 9, no. 4, pp. 4395–4406, Aug. 2021.

[97] M. Mamdouh and M. A. Abido, "Efficient predictive torque control for induction motor drive," *IEEE Trans. Ind. Electron.*, vol. 66, no. 9, pp. 6757–6767, Sep. 2019.

[98] T. Geyer, G. A. Beccuti, G. Papafotiou, and M. Morari, "Model predictive direct torque control of permanent magnet synchronous motors," in *Proc. IEEE Energy Convers. Congr. Expo.*, 2010, pp. 199–206.

[99] T. Geyer, G. Papafotiou, and M. Morari, "Model predictive direct torque control—Part I: Concept, algorithm, and analysis," *IEEE Trans. Ind. Appl.*, vol. 56, no. 6, pp. 1894–1905, Jun. 2009.

[100] J. Holtz, "Predictive finite-state control—When to use and when not," *IEEE Trans. Power Electron.*, vol. 37, no. 4, pp. 4225–4232, Apr. 2022.

[101] H. Makhamreh, M. Sleiman, O. Kukrer, and K. Al-Haddad, "Lyapunov-based model predictive control of a PUC7 grid-connected multilevel inverter," *IEEE Trans. Ind. Electron.*, vol. 66, no. 9, pp. 7012–7021, Sep. 2019.

[102] H. Makhamreh, M. Trabelsi, O. Kukrer, and H. Abu-Rub, "A Lyapunov-based model predictive control design with reduced sensors for a PUC7 rectifier," *IEEE Trans. Ind. Electron.*, vol. 68, no. 2, pp. 1139–1147, Feb. 2021.

[103] A. A. Ahmed, B. K. Koh, and Y. I. Lee, "A comparison of finite control set and continuous control set model predictive control schemes for speed control of induction motors," *IEEE Trans. Ind. Inform.*, vol. 14, no. 4, pp. 1334–1346, Apr. 2018.

[104] R. O. Ramirez, J. R. Espinoza, F. Villarroel, E. Maurelia, and M. E. Reyes, "A novel hybrid finite control set model predictive control scheme with reduced switching," *IEEE Trans. Ind. Electron.*, vol. 61, no. 11, pp. 5912–5920, Nov. 2014.

[105] I. Harbi, M. Ahmed, C. M. Hackl, J. Rodriguez, R. Kennel, and M. Abdelrahem, "Low-complexity dual-vector model predictive control for single-phase nine-level ANPC-based converter," *IEEE Trans. Power Electron.*, vol. 38, no. 3, pp. 2956–2971, Mar. 2022.

[106] D. Schuetz et al., "Space vector modulated model predictive control for grid-tied converters," *IEEE Trans. Ind. Inform.*, vol. 19, no. 1, pp. 414–425, Jan. 2023.

[107] Q. Xiao et al., "Modulated model predictive control for multilevel cascaded H-bridge converter-based static synchronous compensator," *IEEE Trans. Ind. Electron.*, vol. 69, no. 2, pp. 1091–1102, Feb. 2022.

[108] T. Geyer, N. Oikonomou, G. Papafotiou, and F. D. Kieferndorf, "Model predictive pulse pattern control," *IEEE Trans. Ind. Appl.*, vol. 48, no. 2, pp. 663–676, Mar./Apr. 2012.

[109] S. Vazquez et al., "Model predictive control for single-phase NPC converters based on optimal switching sequences," *IEEE Trans. Ind. Electron.*, vol. 63, no. 12, pp. 7533–7541, Dec. 2016.

[110] S. Vazquez, P. Acuna, R. P. Aguilera, J. Pou, J. I. Leon, and L. G. Franquelo, "DC-link voltage-balancing strategy based on optimal switching sequence model predictive control for single-phase H-NPC converters," *IEEE Trans. Ind. Electron.*, vol. 67, no. 9, pp. 7410–7420, Sep. 2020.

[111] Y. Yang, H. Wen, M. Fan, M. Xie, R. Chen, and Y. Wang, "A constant switching frequency model predictive control without weighting factors for T-type single-phase three-level inverters," *IEEE Trans. Ind. Electron.*, vol. 66, no. 7, pp. 5153–5164, Jul. 2019.

[112] P. Karamanakos, T. Geyer, N. Oikonomou, F. D. Kieferndorf, and S. Manias, "Direct model predictive control: A review of strategies that achieve long prediction intervals for power electronics," *IEEE Ind. Electron. Mag.*, vol. 8, no. 1, pp. 32–43, Mar. 2014.

[113] J. Rodriguez et al., "State of the Art of finite control set model predictive control in power electronics," *IEEE Trans. Ind. Inform.*, vol. 9, no. 2, pp. 1003–1016, May 2013.

[114] C. Bordons and C. Montero, "Basic principles of MPC for power converters: Bridging the gap between theory and practice," *IEEE Ind. Electron. Mag.*, vol. 9, no. 3, pp. 31–43, Sep. 2015.

[115] T. Geyer and D. E. Quevedo, "Performance of multistep finite control set model predictive control for power electronics," *IEEE Trans. Power Electron.*, vol. 30, no. 3, pp. 1633–1644, Mar. 2015.

[116] T. Geyer, P. Karamanakos, and R. Kennel, "On the benefit of long-horizon direct model predictive control for drives with LC filters," in *Proc. IEEE Energy Convers. Congr. Expo.*, 2014, pp. 3520–3527.

[117] M. Rossi, E. Liegmann, P. Karamanakos, F. Castelli-Dezza, and R. Kennel, "Long-horizon direct model predictive control for a series-connected modular rectifier," in *Proc. IEEE Int. Exhib. Conf. Power Electron., Intell. Motion, Renewable Energy Energy Manage.*, 2020, pp. 1–8.

[118] M. Rossi, E. Liegmann, P. Karamanakos, F. Castelli-Dezza, and R. Kennel, "Direct model predictive power control of a series-connected modular rectifier," in *Proc. IEEE Int. Symp. Predictive Control Elect. Drives Power Electron.*, 2019, pp. 1–6.

[119] M. Malinowski, K. Gopakumar, J. Rodriguez, and M. A. Perez, "A survey on cascaded multilevel inverters," *IEEE Trans. Ind. Electron.*, vol. 57, no. 7, pp. 2197–2206, Jul. 2010.

[120] M. Rossi, P. Karamanakos, and F. Castelli-Dezza, "Constrained long-horizon direct model predictive control for grid-connected converters with LCL filters," in *Proc. IEEE 24th Eur. Conf. Power Electron. Appl.*, 2022, pp. 1–8.

[121] M. Rossi, P. Karamanakos, and F. Castelli-Dezza, "An indirect model predictive control method for grid-connected three-level neutral point clamped converters with LCL filters," *IEEE Trans. Ind. Appl.*, vol. 58, no. 3, pp. 3750–3768, May/Jun. 2022.

[122] G. Papafotiou, J. Kley, K. G. Papadopoulos, P. Bohren, and M. Morari, "Model predictive direct torque control—Part II: Implementation and experimental evaluation," *IEEE Trans. Ind. Appl.*, vol. 56, no. 6, pp. 1906–1915, Jun. 2009.

[123] T. Geyer, "Computationally efficient model predictive direct torque control," *IEEE Trans. Power Electron.*, vol. 26, no. 10, pp. 2804–2816, Oct. 2011.

[124] T. Geyer, "Model predictive direct current control: Formulation of the stator current bounds and the concept of the switching horizon," *IEEE Ind. Appl. Mag.*, vol. 18, no. 2, pp. 47–59, Mar./Apr. 2012.

[125] P. Karamanakos, T. Geyer, and R. Kennel, "Reformulation of the long-horizon direct model predictive control problem to reduce the computational effort," in *Proc. IEEE Energy Convers. Congr. Expo.*, 2014, pp. 3512–3519.

[126] P. Karamanakos, T. Geyer, and R. P. Aguilera, "Long-horizon direct model predictive control: Modified sphere decoding for transient operation," *IEEE Trans. Ind. Appl.*, vol. 54, no. 6, pp. 6060–6070, Nov./Dec. 2018.

[127] P. Acuña, C. Rojas, R. Baidya, R. P. Aguilera, and J. Fletcher, "On the impact of transients on multistep model predictive control for medium-voltage drives," *IEEE Trans. Power Electron.*, vol. 34, no. 9, pp. 8342–8355, Sep. 2019.

[128] E. Zafra et al., "Parallel sphere decoding algorithm for long-prediction-horizon FCS-MPC," *IEEE Trans. Power Electron.*, vol. 37, no. 7, pp. 7896–7906, Jul. 2022.

[129] F. Grimm, P. Kolahian, Z. Zhang, and M. Baghdadi, "A sphere decoding algorithm for multistep sequential model-predictive control," *IEEE Trans. Ind. Appl.*, vol. 57, no. 3, pp. 2931–2940, May/Jun. 2021.

[130] E. Zafra, S. Vazquez, A. M. Alcaide, L. G. Franquelo, J. I. Leon, and E. P. Martin, "K-Best sphere decoding algorithm for long prediction horizon FCS-MPC," *IEEE Trans. Ind. Electron.*, vol. 69, no. 8, pp. 7571–7581, Aug. 2022.

[131] E. Zafra, S. Vazquez, A. M. Alcaide, E. P. Martin, L. G. Franquelo, and J. I. Leon, "Hybrid sphere decoder for long prediction horizon FCS-MPC," *IEEE Trans. Ind. Electron.*, vol. 70, no. 6, pp. 5484–5492, Jun. 2023.

[132] P. Karamanakos, T. Geyer, and R. Kennel, "Constrained long-horizon direct model predictive control for power electronics," in *Proc. IEEE Energy Convers. Congr. Expo.*, 2016, pp. 1–8.

[133] E. Liegmann, P. Karamanakos, T. Geyer, T. Mouton, and R. Kennel, "Long-horizon direct model predictive control with active balancing of the neutral point potential," in *Proc. IEEE Int. Symp. Predictive Control Elect. Drives Power Electron.*, 2017, pp. 89–94.

[134] F. Grimm, Z. Zhang, F. Wang, and R. Kennel, "Multistep predictive control of three-level NPC converters using weak derivative linearization," in *Proc. Chin. Autom. Congr.*, 2017, pp. 4672–4677.

[135] L. Ortombina, P. Karamanakos, and M. Zigliotto, "Robustness analysis of long-horizon direct model predictive control: Induction motor drives," in *Proc. IEEE 21st Workshop Control Model. Power Electron.*, 2020, pp. 1–8.

[136] L. Ortombina, P. Karamanakos, and M. Zigliotto, "Robustness analysis of long-horizon direct model predictive control: Permanent magnet synchronous motor drives," in *Proc. IEEE 21st Workshop Control Model. Power Electron.*, 2020, pp. 1–8.

[137] A. Tregubov, P. Karamanakos, and L. Ortombina, "A computationally efficient robust direct model predictive control for medium voltage induction motor drives," in *Proc. IEEE Energy Convers. Congr. Expo.*, 2021, pp. 4690–4697.

[138] M. Dorfling, H. Mouton, P. Karamanakos, and T. Geyer, "Experimental evaluation of sphere decoding for long-horizon direct model predictive control," in *Proc.IEEE Eur. Power Electron. Conf.*, 2017, pp. P.1–P.10.

[139] M. Dorfling, H. Mouton, T. Geyer, and P. Karamanakos, "Long-horizon finite-control-set model predictive control with non-recursive sphere decoding on an FPGA," *IEEE Trans. Power Electron.*, vol. 35, no. 7, pp. 7520–7531, Jul. 2020.

[140] S. A. B. Khalid, E. Liegmann, P. Karamanakos, and R. Kennel, "High-level synthesis of a long horizon model predictive control algorithm for an FPGA," in *Proc. IEEE Int. Exhib. Conf. Power Electron., Intell. Motion, Renew. Energy Energy Manage.*, 2020, pp. 1544–1551.

[141] E. Liegmann, T. Schindler, P. Karamanakos, A. Dietz, and R. Kennel, "UltraZohm—An open-source rapid control prototyping platform for power electronic systems," in *Proc. IEEE Int. Aegean Conf. Elect. Mach. Power Electron./Int. Conf. Optim. Elect. Electron. Equip.*, 2021, pp. 445–450.

[142] E. Liegmann, P. Karamanakos, and R. Kennel, "Implementation of a long-horizon model predictive control algorithm on an embedded system," in *Proc. 23rd Eur. Conf. Power Electron. Appl.*, 2021, pp. P.1–P.10.

[143] E. Liegmann, P. Karamanakos, and R. Kennel, "Real-time implementation of long-horizon direct model predictive control on an embedded system," *IEEE Open J. Ind. Appl.*, vol. 3, pp. 1–12, 2022.

[144] R. Baidya, R. P. Aguilera, P. Acuña, S. Vasquez, and H. du Toit Mouton, "Multistep model predictive control for cascaded H-bridge inverters—Formulation and analysis," *IEEE Trans. Power Electron.*, vol. 33, no. 1, pp. 876–886, Jan. 2018.

[145] A. Andersson and T. Thiringer, "Assessment of an improved finite control set model predictive current controller for automotive propulsion applications," *IEEE Trans. Ind. Electron.*, vol. 67, no. 1, pp. 91–100, Jan. 2020.

[146] P. Karamanakos, T. Geyer, and R. Kennel, "A computationally efficient model predictive control strategy for linear systems with integer inputs," *IEEE Trans. Control Syst. Technol.*, vol. 24, no. 4, pp. 1463–1471, Jul. 2016.

[147] J.-Z. Zhang, T. Sun, F. Wang, J. Rodríguez, and R. Kennel, "A computationally efficient quasi-centralized DMPC for back-to-back converter PMSG wind turbine systems without dc-link tracking errors," *IEEE Trans. Ind. Appl.*, vol. 63, no. 10, pp. 6160–6171, Oct. 2016.

[148] M. Siami, D. A. Khaburi, M. Rivera, and J. Rodríguez, "A computationally efficient lookup table based FCS-MPC for PMSM drives fed by matrix converters," *IEEE Trans. Ind. Appl.*, vol. 64, no. 10, pp. 7645–7654, Oct. 2017.

[149] Y. Zhang, B. Zhang, H. Yang, M. Norambuena, and J. Rodriguez, "Generalized sequential model predictive control of IM drives with field-weakening ability," *IEEE Trans. Power Electron.*, vol. 34, no. 9, pp. 8944–8955, Sep. 2019.

[150] G. Mirzaeva, G. C. Goodwin, B. P. McGrath, C. Teixeira, and M. E. Rivera, "A generalized MPC framework for the design and comparison of VSI current controllers," *IEEE Trans. Ind. Appl.*, vol. 63, no. 9, pp. 5816–5826, Sep. 2016.

[151] S. Kwak and J. C. Park, "Switching strategy based on model predictive control of VSI to obtain high efficiency and balanced loss distribution," *IEEE Trans. Power Electron.*, vol. 29, no. 9, pp. 4551–4567, Sep. 2014.

[152] M. P. Akter, S. Mekhilef, N. M. L. Tan, and H. Akagi, "Modified model predictive control of a bidirectional ac-dc converter based on Lyapunov function for energy storage systems," *IEEE Trans. Ind. Electron.*, vol. 63, no. 2, pp. 704–715, Feb. 2016.

[153] H. Komurcugil, N. Guler, and S. Bayhan, "Weighting factor free Lyapunov-function-based model predictive control strategy for single-phase T-type rectifiers," in *Proc. IEEE 46th Annu. Conf. Ind. Electron. Soc.*, 2020, pp. 4200–4205.

[154] N. Guler and H. Komurcugil, "Energy function based finite control set predictive control strategy for single-phase split source inverters," *IEEE Trans. Ind. Electron.*, vol. 69, no. 6, pp. 5669–5679, Jun. 2022.

[155] A. M. Dadu, T. K. Soon, S. Mekhilef, and M. Nakaoka, "Lyapunov law based model predictive control scheme for grid connected three phase three level neutral point clamped inverter," in *Proc. IEEE 3rd Int. Future Energy Electron. Conf. ECCE Asia*, 2017, pp. 512–516.

[156] X. Liu, D. Wang, and Z. Peng, "A computationally efficient FCS-MPC method without weighting factors for NNPCs with optimal duty cycle control," *IEEE/ASME Trans. Mechatron.*, vol. 23, no. 5, pp. 2503–2514, Oct. 2018.

[157] X. Liu et al., "Lyapunov-based finite control-set model predictive control for nested neutral point-clamped converters without weighting factors," *Int. J. Elect. Power Energy Syst.*, vol. 121, 2020, Art. no. 106071.

[158] G. Prior and M. Krstic, "A control Lyapunov approach to finite control set model predictive control for permanent magnet synchronous motors," *J. Dyn. Syst., Meas. Control*, vol. 137, 2015, Art. no. 011001.

[159] H. T. Nguyen and J. W. Jung, "Finite control set model predictive control to guarantee stability and robustness for surface-mounted PM synchronous motors," *IEEE Trans. Ind. Electron.*, vol. 65, no. 11, pp. 8510–8519, Nov. 2018.

[160] M. Preindl, "Robust control invariant sets and Lyapunov-based MPC for IPM synchronous motor drives," *IEEE Trans. Ind. Electron.*, vol. 63, no. 6, pp. 3925–3933, Jun. 2016.

[161] G. Q. Bao, W. Qi, and T. He, "Direct torque control of PMSM with modified finite set model predictive control," *Energies*, vol. 13, 2020, Art. no. 234.

[162] B. Babaghorbani, M. T. Beheshti, and H. A. Talebi, "A Lyapunov-based model predictive control strategy in a permanent magnet synchronous generator wind turbine," *Int. J. Elect. Power Energy Syst.*, vol. 130, 2021, Art. no. 106972.

[163] H. Komurcugil, S. Bayhan, N. Guler, and F. Blaabjerg, "An effective model predictive control method with self-balanced capacitor voltages for single-phase three-level shunt active filters," *IEEE Access*, vol. 9, pp. 103811–103821, 2021.

[164] X. Liu et al., "Lyapunov-based fast finite-state model predictive control for sensorless three-phase four-arm MMC," *IEEE Trans. Emerg. Sel. Topics Power Electron.*, vol. 11, no. 3, pp. 2930–2941, Jun. 2023.

[165] S. Boyd and L. Vandenberghe, *Convex Optimization*. Cambridge, U.K.: Cambridge Univ. Press, 2004.

[166] J. Ma, W. Song, S. Wang, and X. Feng, "Model predictive direct power control for single phase three-level rectifier at low switching frequency," *IEEE Trans. Power Electron.*, vol. 33, no. 2, pp. 1050–1062, Feb. 2018.

[167] J. Yin, J. I. Leon, M. A. Perez, L. G. Franquelo, A. Marquez, and S. Vazquez, "Model predictive control of modular multilevel converters using quadratic programming," *IEEE Trans. Power Electron.*, vol. 36, no. 6, pp. 7012–7025, Jun. 2021.

[168] M. Urrutia, R. Cárdenas, J. C. Clare, and A. Watson, "Circulating current control for the modular multilevel matrix converter based on model predictive control," *IEEE J. Emerg. Sel. Topics Power Electron.*, vol. 9, no. 5, pp. 6069–6085, Oct. 2021.

[169] E. Rodriguez, R. Leyva, C. D. Townsend, G. G. Farivar, H. D. Tafti, and J. Pou, "Constrained control of low-capacitance delta cascaded H-bridge StatComs: A model predictive control approach," *IEEE Trans. Power Electron.*, vol. 36, no. 12, pp. 14312–14328, Dec. 2021.

[170] K. Bándy and P. Stumpf, "Quadratic regression model based indirect model predictive control of ac drives," *IEEE Trans. Power Electron.*, vol. 37, no. 11, pp. 13158–13177, Nov. 2022, doi: 10.1109/TPEL.2022.3181749.

[171] A. M. Lopez, D. E. Quevedo, R. P. Aguilera, T. Geyer, and N. Oikonomou, "Limitations and accuracy of a continuous reduced-order model for modular multilevel converters," *IEEE Trans. Power Electron.*, vol. 33, no. 7, pp. 6292–6303, Jul. 2018.

[172] E. F. Camacho and C. Bordons, *Model Predictive Control*. London, U.K.:Springer, 2007.

[173] Y. Tajima, Y. Hori, T. Ino, T. Yokoyama, L. Ben-Brahim, and M. Trabelsi, "Deadbeat control with multi-sampling compensation for medium-voltage motor drives by cascaded multi-cell inverter using FPGA based hardware controller," in *Proc. IEEE 8th Int. Conf. Power Electron.*, 2011, pp. 2492–2497.

[174] M. Trabelsi, L. Ben-Brahim, A. Gastli, and H. Abu-Rub, "Enhanced deadbeat control approach for grid-tied multilevel flying capacitors inverter," *IEEE Access*, vol. 10, pp. 16720–16728, 2022.
[175] X. Chen, J. Liu, S. Song, and S. Ouyang, "Circulating harmonic currents suppression of level-increased NLM based modular multilevel converter with deadbeat control," *IEEE Trans. Power Electron.*, vol. 35, no. 11, pp. 11418–11429, Nov. 2020.
[176] M.-H. Jahanbakhshi, B. Asaei, and B. Farhangi, "A novel deadbeat controller for single phase PV grid connected inverters," in *Proc. IEEE 23rd Iranian Conf. Elect. Eng.*, 2015, pp. 1613–1617.
[177] G. Buticchi, D. Barater, L. Tarisciotti, and P. Zanchetta, "A simple deadbeat current control for single-phase transformerless inverters with LCL filter," in *Proc. IEEE Energy Convers. Congr. Expo.*, 2013, pp. 4214–4220.
[178] J. Wang, Y. Song, and A. Monti, "Design of a high performance deadbeat-type current controller for LCL-filtered grid-parallel inverters," in *Proc. IEEE 6th Int. Symp. Power Electron. Distrib. Gener. Syst.*, 2015, pp. 1–8.
[179] M. R. P. Kumar and J. Kim, "Dead-beat control of hybrid multilevel switching converter," in *Proc. IEEE 27th Annu. Power Electron. Spec. Conf.*, 1996, pp. 782–788.
[180] S. Ramaiah, N. Lakshminarasamma, and M. K. Mishra, "An improved deadbeat direct power control for grid connected inverter system," in *Proc. IEEE 12th Int. Symp. Power Electron. Distrib. Gener. Syst.*, 2021, pp. 1–6.
[181] M. Abarzadeh, K. Al-Haddad, and M. R. Dehbozorgi, "Deadbeat predictive direct power control of neutral-point-clamped converter based active front end rectifier for more electric aircraft applications," in *Proc. IEEE 44th Annu. Conf. Ind. Electron. Soc.*, 2018, pp. 5739–5744.
[182] J. Wang, Y. Tang, P. Lin, X. Liu, and J. Pou, "Deadbeat predictive current control for modular multilevel converters with enhanced steady-state performance and stability," *IEEE Trans. Power Electron.*, vol. 35, no. 7, pp. 6878–6894, Jul. 2020.
[183] T. Dragicevic, "Model predictive control of power converters for robust and fast operation of ac microgrids," *IEEE Trans. Power Electron.*, vol. 33, no. 7, pp. 6304–6317, Jul. 2018.
[184] M. Novak and T. Dragicevic, "Supervised imitation learning of finite-set model predictive control systems for power electronics," *IEEE Trans. Ind. Electron.*, vol. 68, no. 2, pp. 1717–1723, Feb. 2021.
[185] T. Dragicevic, S. Vazquez, and P. Wheeler, "Advanced control methods for power converters in DG systems and microgrids," *IEEE Trans. Ind. Electron.*, vol. 68, no. 7, pp. 5847–5862, Jul. 2021.
[186] C. Zheng, T. Dragičević, B. Majmunović, and F. Blaabjerg, "Constrained modulated model-predictive control of an LC-filtered voltage-source converter," *IEEE Trans. Power Electron.*, vol. 35, no. 2, pp. 1967–1977, Feb. 2020.
[187] B. Majmunovic, T. Dragicevic, and F. Blaabjerg, "Multi objective modulated model predictive control of stand-alone voltage source converters," *IEEE Trans. Emerg. Sel. Topics Power Electron.*, vol. 8, no. 3, pp. 2559–2571, Sep. 2020.
[188] S. A. Khan, Y. Guo, Y. P. Siwakoti, D. D.-C. Lu, and J. Zhu, "A disturbance rejection-based control strategy for five-level T-type hybrid power converters with ripple voltage estimation capability," *IEEE Trans. Ind. Electron.*, vol. 67, no. 9, pp. 7364–7374, Sep. 2020.
[189] S. Vazquez, E. Zafra, R. P. Aguilera, T. Geyer, J. I. Leon, and L. G. Franquelo, "Prediction model with harmonic load current components for FCS-MPC of an uninterruptible power supply," *IEEE Trans. Power Electron.*, vol. 37, no. 1, pp. 322–331, Jan. 2022.
[190] M. S. Mousavi, S. A. Davari, V. Nekoukar, C. Garcia, and J. Rodriguez, "Integral sliding mode observer-based ultralocal model for finite-set model predictive current control of induction motor," *IEEE Trans. Emerg. Sel. Topics Power Electron.*, vol. 10, no. 3, pp. 2912–2922, Jun. 2022.
[191] X. Liu et al., "Predictor-based neural network finite-set predictive control for modular multilevel converter," *IEEE Trans. Ind. Electron.*, vol. 68, no. 11, pp. 11621–11627, Nov. 2021.
[192] X. Liu, L. Qiu, Y. Fang, K. Wang, Y. Li, and J. Rodríguez, "A fuzzy approximation for FCS-MPC in power converters," *IEEE Trans. Power Electron.*, vol. 37, no. 8, pp. 9153–9163, Aug. 2022.
[193] M. Novak, U. M. Nyman, T. Dragicevic, and F. Blaabjerg, "Analytical design and performance validation of finite set MPC regulated power converters," *IEEE Trans. Ind. Electron.*, vol. 66, no. 3, pp. 2004–2014, Mar. 2019.
[194] J. Holtz, "Pulsewidth modulation for electronic power conversion," *Proc. IEEE*, vol. 82, no. 8, pp. 1194–1214, Aug. 1994.
[195] M. Easley, M. B. Shadmand, and H. Abu-Rub, "Computationally-efficient optimal control of cascaded multilevel inverters with power balance for energy storage systems," *IEEE Trans. Ind. Electron.*, vol. 68, no. 12, pp. 12285–12295, Dec. 2021.
[196] A. Mora, R. Cardenas, R. P. Aguilera, A. Angulo, P. Lezana, and D. D.-C. Lu, "Predictive optimal switching sequence direct power control for grid-tied 3L-NPC converters," *IEEE Trans. Ind. Electron.*, vol. 68, no. 9, pp. 8561–8571, Sep. 2021.

Ibrahim Harbi (Member, IEEE) received the B.Sc. (Hons.) and M.Sc. degrees in electrical engineering from Menoufia University, Shebin El-Koum, Egypt, in 2012 and 2016, respectively. He is currently working toward the Dr. Ing. degree in electrical engineering with the Chair of High-Power Converter Systems, Technical University of Munich, Munich, Germany.

His research interests include multilevel converters topologies and predictive control of power electronics converters.

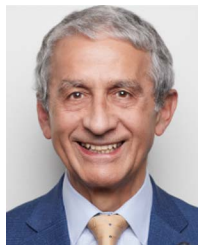

Jose Rodriguez (Life Fellow, IEEE) received the Engineer degree in electrical engineering from the Universidad Tecnica Federico Santa Maria, Valparaíso, Chile, in 1977, and the Dr.-Ing. degree in electrical engineering from the University of Erlangen, Erlangen, Germany, in 1985.

From 2015 to 2019, he was the President of Universidad Andres Bello, Santiago, Chile. Since 2022, he has been the President of Universidad San Sebastian, Santiago. His main research interests include multilevel inverters, new converter topologies, control of power converters, and adjustable-speed drives.

Eyke Liegmann (Student Member, IEEE) received the B.Sc. and M.Sc. degrees in electrical engineering from RWTH Aachen University, Aachen, Germany, in 2013 and 2016, respectively. He is currently working toward the Dr.Ing. degree in electrical engineering with the Technical University of Munich, Munich, Germany.

His research interests include field-programmable-gate-array-based control systems and model-predictive control of electrical drive systems.

Hamza Makhamreh received the Ph.D. degree in electrical and electronic engineering from Eastern Mediterranean University, Famagusta, Cyprus, in 2019.

He is currently a Faculty Member with Özyeğin University, Istanbul, Turkey, specializing in power electronics control, including model-predictive control and Lyapunov-based finite-set model-predictive control for various applications.

Marcelo Lobo Heldwein (Senior Member, IEEE) received the B.S. and M.S. degrees in electrical engineering from the Federal University of Santa Catarina, Florianópolis, Brazil, in 1997 and 1999, respectively, and the Ph.D. degree in electrical engineering from the Swiss Federal Institute of Technology, Zurich, Switzerland, in 2007.

He is currently the Head of the Chair of High-Power Converter Systems, Technical University of Munich, Munich, Germany. His research interests include power electronics converters and electromagnetic compatibility.

Mateja Novak (Member, IEEE) received the M.Sc. degree in electrical engineering and information technology from the University of Zagreb, Zagreb, Croatia, in 2014, and the Ph.D. degree in electrical engineering from Aalborg University, Aalborg, Denmark, in 2020.

She is currently a Postdoctoral Researcher with AAU Energy, Aalborg University. Her research interests include predictive control, multilevel converters, deep learning, statistical model checking, and reliability of power electronic systems.

Mattia Rossi (Member, IEEE) received the B.Sc. and M.Sc. degrees in automation and control engineering from the Politecnico di Milano, Milan, Italy, in 2013 and 2015, respectively, and the Ph.D. degree in electrical engineering from the Politecnico di Milano, in collaboration with Tampere University, Tampere, Finland, in 2021.

He is currently a Postdoctoral Research Fellow with the Faculty of Information Technology and Communication Sciences, Tampere University. His main research interests include formulation and embedded implementation of predictive control for power-electronic-based systems and system component reliability.

Mohamed Abdelrahem (Senior Member, IEEE) received the B.Sc. (Hons.) and M.Sc. degrees in electrical engineering from Assiut University, Asyut, Egypt, in 2007 and 2011, respectively, and the Ph.D. (Hons.) degree in electrical engineering from the Technical University of Munich (TUM), Munich, Germany, in 2020.

Since 2019, he has been the Head of the Renewable Energy Systems Research Group, Chair of High-Power Converter Systems, TUM. Since 2020, he has also been an Assistant Professor with the Department of Electrical Engineering, Assiut University. His research interests include power electronics, predictive and encoderless control of variable-speed wind generators, and photovoltaic systems.

Mohamed Trabelsi (Senior Member, IEEE) received the B.Sc. degree in electrical engineering from the National Institute of Applied Sciences and Technology, Tunis, Tunisia, in 2006, and the M.Sc. degree in automated systems and the Ph.D. degree in energy systems from INSA Lyon, Villeurbanne, France, in 2006 and 2009, respectively.

In September 2018, he joined the Kuwait College of Science and Technology, Kuwait City, Kuwait, as an Associate Professor, where he is currently a Full Professor. His research interests include control systems with applications arising in the contexts of power electronics, energy conversion, renewable energies integration, and smart grids.

Mostafa Ahmed (Member, IEEE) received the B.Sc. (Hons.) and M.Sc. degrees in electrical engineering from Assiut University, Asyut, Egypt, in 2010 and 2015, respectively. He is currently working toward the Dr.Ing. degree in electrical engineering with the Chair of High-Power Converter Systems, Technical University of Munich, Munich, Germany.

His research interests include renewable energy systems, modeling of photovoltaic systems, and predictive control of power electronics converters.

Petros Karamanakos (Senior Member, IEEE) received the Diploma and Ph.D. degree in electrical and computer engineering from the National Technical University of Athens, Athens, Greece, in 2007, and 2013, respectively.

Since 2016, he has been with the Faculty of Information Technology and Communication Sciences, Tampere University, Tampere, Finland, where he is currently an Associate Professor. His main research interests include intersection of optimal control, mathematical programming, and power electronics, including model-predictive control and optimal modulation for utility-scale power converters and ac variable-speed drives.

Shuai Xu (Member, IEEE) received the Ph.D. degree in electrical engineering from Southeast University, Nanjing, China, in 2018.

From 2016 to 2017, he was a joint Ph.D. student with the University of British Columbia, Vancouver, BC, Canada. Since 2019, he has been with the State Key Laboratory of Rail Transit Vehicle System, Southwest Jiaotong University, Chengdu, China. His research interests include advanced control of multilevel power converters, motor drives, and fault diagnosis and fault-tolerant control.

Tomislav Dragičević (Senior Member, IEEE) received the M.Sc. and Industrial Ph.D. degrees in electrical engineering from the Faculty of Electrical Engineering, University of Zagreb, Zagreb, Croatia, in 2009 and 2013, respectively.

He is currently a Professor with the Technical University of Denmark, Lyngby, Denmark, where he leads research in the digitization of power converters. His research interests include application of advanced control, optimization, and artificial-intelligence-inspired techniques.

Ralph Kennel (Senior Member, IEEE) received the Diploma and Dr.-Ing. degrees in electrical engineering from the University of Kaiserslautern, Kaiserslautern, Germany, in 1979 and 1984, respectively.

Since 2008, he has been a Professor of Electrical Drive Systems and Power Electronics with the Technical University of Munich, Munich, Germany. His main research interests include sensorless control of ac drives, predictive control of power electronics, and hardware-in-the-loop systems.